Thesis for Master's Degree

A Radar Electronic Surveillance System Using a Sub-Nyquist Receiver

Jeong Park

School of Electrical Engineering and Computer Science

Gwangju Institute of Science and Technology

2017

석 사 학 위 논 문

Sub-Nyquist 수신기를 이용한 레이더 전자 감시 체계

박 정

전 자 전 기 컴 퓨 터 공 학 부

광 주 과 학 기 술 원

2017

A Radar Electronic Surveillance System Using a Sub-Nyquist Receiver

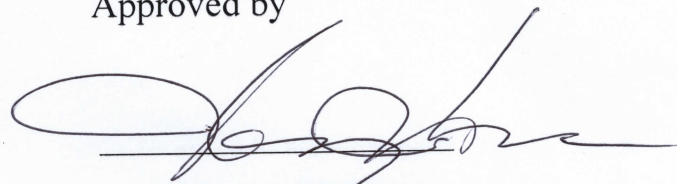Advisor: Heung-No Lee

by

Jeong Park

School of Electrical Engineering and Computer Science

Gwangju Institute of Science and Technology

A thesis submitted to the faculty of the Gwangju Institute of Science and Technology in partial fulfillment of the requirements for the degree of Master of Science in the School of Electrical Engineering and Computer Science

Gwangju, Republic of Korea

2017. 11. 30

Approved by

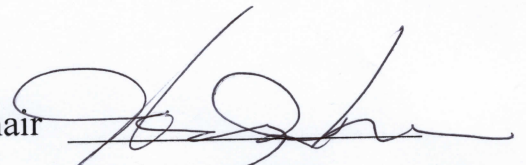Professor Heung-No Lee

Committee Chair

A Radar Electronic Surveillance System Using a Sub-Nyquist Receiver

Jeong Park

Accepted in partial fulfillment of the requirements for the
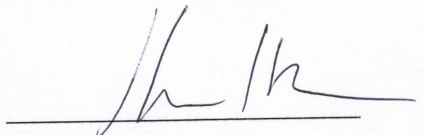
degree of Master of Science
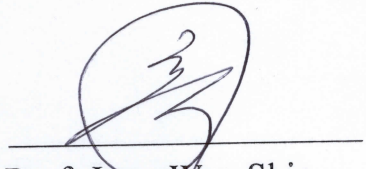
November   30th   2017

Committee Chair _____

Prof. Heung-No Lee

Committee Member _____

Prof. Kiseon Kim

Committee Member _____

Prof. Jong Won Shin

Abstract

In this paper, we aim to propose a new radar electronic surveillance (ES) system with sub-Nyquist monitoring capacity and its calibration algorithm. The system acquires the radar signals from unknown sources by sampling the signals at a rate below the Nyquist rate. The modulated wideband converter (MWC) is well known for a sub-Nyquist sampling wideband receiver system, based on the compressed sensing (CS) theory. The radar ES system makes use of MWC for very wideband electronic surveillance. However, the previous MWC, for the radar signals, holds a high computational complexity in the post processing. The proposed radar ES system, including a preprocessing method for the following CS recovery algorithm reduces the computational complexities. Before designing the radar ES system, in this paper, we start with summarizing some wideband signal receivers and providing a probability analysis about signal acquiring performances of the sub-Nyquist receivers including the conventional Nyquist receiver, which is clear and straightforward analysis. In the latter of paper, to estimate practical system transfer of the MWC, we provide calibration algorithms, which should be conducted when the MWC is implemented in the real world.

Contents

List of Figures

List of Tables

I. Introduction

The radar electronic surveillance (ES) system acquires priorly unknown wideband radar signals emitted from opponent radar system, as shown in Fig.1. The signal is generated from opponent radar system, which notifies subject by transmitting radar signal and receiving the its reflection from the subjects. The Fig.2. depicts the signal of interest, which laid in a wideband and exist as spectrally sparse signal. The radar ES system is useful for recognizing the intent of the treat in advance.
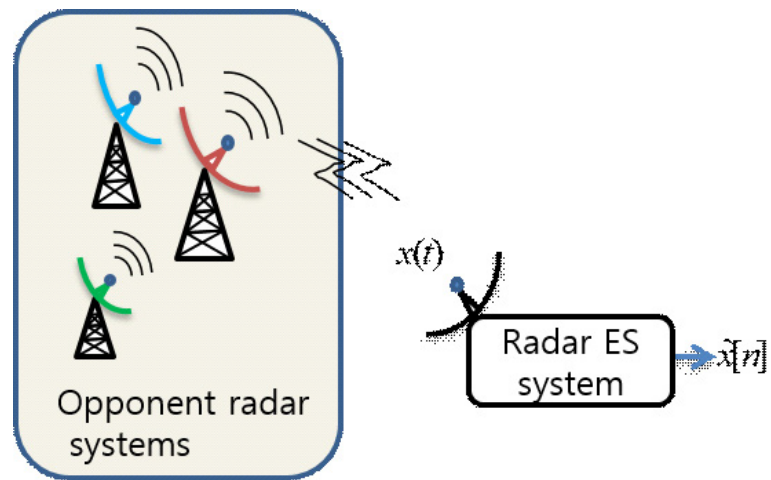
Fig. 1. The concept figure of radar electronic surveillance system.
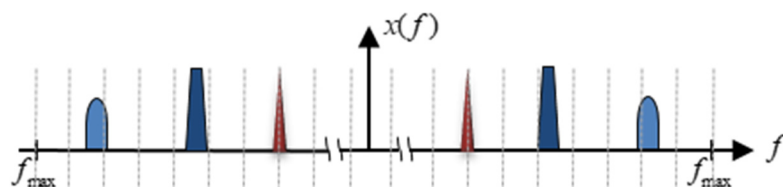
Fig. 2. An aggregation of wideband radar signals.

The radar ES system makes use of a certain signal receiver including analog-to digital converter (ADC). The ADC generally becomes an obstacle to sample wideband signals. To avoid aliasing problem, the ADC should sample the signal at the Nyquist rate, which is double of the maximum frequency. However, although recent sampling rate [1] of ADC can cover the wideband range as number of Giga hertz, to arrange the Nyquist ADC is almost impractical. The high sampling rate of ADC yields high power supply and memory problem.

The radar ES system can make use of a Nyquist receiver, such as the rapidly swept super-heterodyne receiver (RSSR) [2], [22] . The RSSR sampled subbands of the wideband region chronologically. However, the RSSR inevitably omitted the signals. For the wideband signals, sweeping period also was widened whereas signal existing time is short. As shown in Fig.3, although a signal exists in some subbands for a while, the RSSR just samples empty subbands while omitting the signal. The inevitable omission of the RSSR becomes a critical problem depending on application, e.g. detection missile or hostile aircraft.
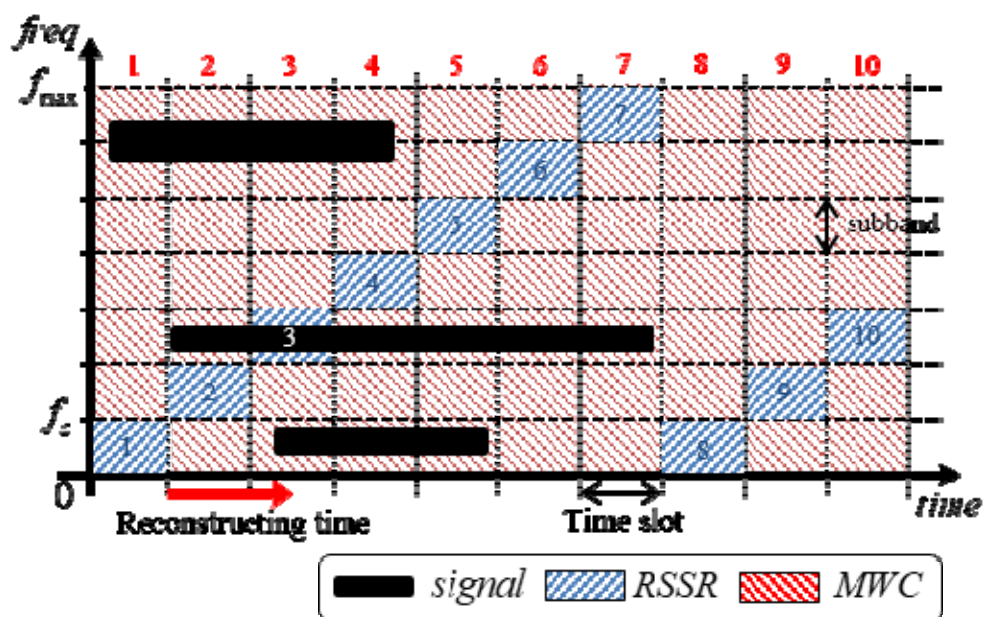
Fig. 3. Signal model and signal acquisition schemes of the RSSR and MWC respectively denoted as blue and red colored integers.

The theory of compressive sensing (CS) [3], [4] provides an alternative solution, sub-Nyquist receiver. The theory suggests that spectrally sparse signals, which contain a small amount of information across a wideband spectrum, can be sampled at a low rate far below the Nyquist rate, and then reconstructed from the samples without losses. Based on the CS, researchers in the past have developed sub-Nyquist receivers, including the modulated wideband converter (MWC) [5], [21], random demodulator[6], multi-coset sampler [7], [8], compressive multiplexer [9], multirate sampler[10], and random modulation pre-integration (RMPI) [11], [12].

Among the sub-Nyquist receivers, the RMPI [11], [12] was inappropriate to be employed to acquire radar signals, since it yielded excessively long computing time and only permitted a small number of signals. The dimension of their system matrix was too huge. The reason of huge system matrix is the system model of the RMPI densely discretized continuous spectrum. For the reconstruction by CS recovery algorithms, it needed excessively high computational complexity (CC), which enlarges computing time. What's more, the sample vector had a large number of non-zero entries per a signal, i.e. the sparsity of the vector is high. The ability to recover the signals with a CS algorithm is restricted as a function of sparsity [13]. Hence, the RMPI took a long time to recover the signals with a CS algorithm or only a small number of radar signals could be acquired.

The MWC [5], [21] overcomes the problems of the RMPI. After sub-Nyquist sampling in the analog part, the reconstruction process is concluded to digital signal processing (DSP) and a CS recovery algorithm. In the DSP, the number of the sample sequences, corresponding to the number of analog channels, is increased through digital filtering and convolutions. The increased number of sequences gives enlarged evidence to recover the signals with the post CS recovery algorithm. In the CS algorithm, the MWC requires low CC compared to the RMPI. For instant, size of the system matrix is the number of increased analog channels by subbands. For the same signal, the sparsity of the spectrum is also smaller than the RMPI. In addition, the MWC is one of realizable sub-Nyquist receivers. The hardware of MWC was realized by Eldar [5], and they demonstrated the success of acquiring the wideband signals. These pros make that the MWC is considered to be employed for the radar ES system.

Although the MWC is regarded as one of most realizable and efficient sub-Nyquist receiver, the signal acquiring performance of the MWC was not analyzed. The benefit of sub-Nyquist MWC, in terms of the performance, even was not verified to the conventional Nyquist receiver with same amount of hardware cost. In addition, the signal acquisition performances of sub-Nyquist receivers were not compared through an analysis. To compare the performances, it may be considered to body out all the receivers and run hundred times. However, it is very inefficient and impractical method. Thus, a comparative analysis which can be used to verify the acquisition performance with a similar realization cost is needed.

A high CC of the MWC yielded from long observing time is critical problem in many ways. Due to tactical purpose such as avoidance of reverse-trace by the enemy, the modern radar system switches their radar signal characteristics. To capture the radar signals, a long observation time is required. However, there are a lot of samples proportional to the observation time. From the convolution process in the DSP, the large number v of samples rapidly increases CC as $O(v^2)$, explained at Section II-D.

In addition, for a given Nyquist frequency and observation time, another factor increasing CC is unnecessarily large size matrices exploited in the post CS recovery algorithm. When the MWC observes and reconstructs signals simultaneously, the high CCs pose bottle-neck phenomenon. The bottle-neck phenomenon corresponds to failure in continuous signal acquisition, since the reconstruction process cannot be completed within the observation period. Thus, to avoid that, reducing CC in the reconstruction process is required.

The theoretical studies on the MWC usually assume that the analog components are ideal and delays do not exist amongst analog components. However, when the MWC is implemented in real world, the assumptions are not valid. This invalid assumption causes model-mismatch problems leading to failure in the reconstruction of Nyquist samples. Thus, calibration techniques for remedying the problems are required for the successful reconstruction.

For the calibration of MWC, researchers have proposed schemes sequentially injecting sinusoids [14]–[17]. In [14], the authors have considered non-linearity of mixer and non-ideal response of filters.

In [15], the authors have considered perturbations of ADC. From an assumption the perfect synchronization between the mixer and the ADC, they derive useful information and exploit it to the calibration. However, the perfect synchronization requires additional electronic parts, which might be complex and highly costs to be implemented for fast ADC. In [16], they have considered the delays in analog paths and difference among channel gains. In [17], the authors have considered a problem of non-ideal LPF. Consequently, all the literatures of [14]–[17] solve their own problems by injecting arbitrarily generated sinusoids with assuming that the phases of the sinusoids are perfectly controllable. However, the phases may be unknown in practice due to the unknown transient between the sinusoid generator and the front-end of the MWC, and the unknown phases again result in the failure in the reconstruction. For the more precise calibration, we need to estimate the phases of sinusoids injected for the calibration.

This paper is summarized as a signal acquisition analysis, radar ES system, and calibration methods for the MWC. The probability analysis to compare the signal acquisition performances of wideband signal receivers is firstly presented. Without implementing all the receivers and operating hundreds of times, we could compare the performances. The analysis demonstrated amount of benefit of the MWC compared to the conventional RSSR. In addition, the analysis could be applied to the other sub-Nyquist receivers based on the CS, and we adopt the RMPI as the example. In addition, the analysis could give a guide to design system parameters of the following radar ES system. Second, with the MWC, we propose a radar ES system to monitor radar signals with reduced CCs. To reduce CCs in the reconstruction process, we propose a time division scheme with a DSP method and a low complexity CS recovery algorithm. By dividing observation time into several timeslots and processing them separately through the DSP, we could reduce overall CC. However, synthesizing the timeslots to revert them as the original observation time caused increases of reconstruction error at borders of the time slots. To alleviate the problem, we provide a solution and verify the effect of it through simulations. After the DSP, we provide a preprocessing method for the following CS recovery algorithm. The method could extract essential measurement vectors without missing signal information to reduce CC of the following recovery algorithm while keeping similar reconstruction performance. Consequently, the

radar ES system with the preprocessing method could relieve much burden of CCs. At last, we propose a calibration algorithm for the MWC sequentially injecting sinusoids with unknown phases. In addition to considering the implementation problems from the non-ideality of the analog parts, we consider that the phases of the sinusoids injected during the calibration are unknown and not consistent for every calibration. In the proposed algorithms, the unknown phases and the calibrated transfer function are estimated at the same time. The estimation of the unknown phases is fulfilled by simple multiplications and divisions, and it is easy to be implemented

The outline of this paper is as follows. Section II briefly introduces the wideband signal receivers including RSSR, RMPI, and MWC, and there is an analysis about *noise folding* problem in the MWC. Section III provides a probability analysis of signal acquisition between the receivers. Section IV presents the sub-Nyquist radar ES system: the time division scheme, the DSP, and the synthetization process, and a low complexity algorithm based on the SOMP. Several calibration methods are given in section V. Section VI concludes this paper.

II. Wideband Signal Receivers

Throughout our study, our goal was to acquire successively incoming wideband radar signals for the ES. The input $x(t)$ is an aggregation of radar signals generated from different radar systems. Specifically, the input is defined by

$$x(t) = \sum_{i=1}^{N} r_i(t), \ 0 \leq t < \infty \qquad (1)$$

where $r_i(t)$ is a radar signal from the i-th radar system and is widely located within $\mathcal{F}_{NYQ} = [-f_{max}, f_{max}]$ where f_{max} is up to scores of Giga-Hertz. Including the carrier frequencies, the pulse description words (PDW) such as PRI, the time of arrivals (TOA), the time of departures (TOD), pulse widths, and the duty cycles are unknown a priori. For every $r_i(t)$, we model the carrier frequency ranges within $[0, f_{max})$, and the bandwidth B_i is truncated to $B_{min} \leq B_i \leq B_{max}$. For separable $r_i(t)$, we assume the spectra of $r_i(t)$ are disjoint with each other. In addition, the aggregation $x(t)$ is sparse in the frequency domain, i.e., $2NB_{max} \ll f_{max}$. Briefly, we acquire a successively incoming signal $x(t)$, which is regarded as a spectrally sparse multiband signal [21] with unknown parameters.

2.1. The Rapid Swept Super-heterodyne Receiver (RSSR)

In this section, we briefly introduce the RSSR [22]. The RSSR receives a multiband signal and divides the whole range of the spectrum into multiple segments, exploiting a bank of bandpass filters (BPFs), and then the segments are sampled by an analog-to digital converter (ADC). According to time-division multiplex [2], the RSSR acquires all the segments chronologically. In other words, the RSSR sequentially acquires the segments one by one, consuming a certain time per each segmented band.

However, the RSSR inevitably omits some spectra of the incoming signals owing to the time-division multiplexing. While the RSSR acquires several segments, the spectra in the remaining bands disappear

or are replaced by others. As the number of signals and/or the range of the input spectrum increases, the omission gets worse. In section III, we present an analysis of signal acquiring rate and verify the omission

2.2. Random Modulated Pre-Integer (RMPI)

The RMPI [11] is one of channelized sub-Nyquist receiver, which acquires a multiband signal for an observation time T_o. For a channel, the multiband signal is mixed with a pseudo random (PR) sequence and the mixed result is then integrated. An ADC after the integrating part samples the mixed result at a sub-Nyquist rate f_s. By denoting m as the number of channel, the channel-end sampling rate [12] f_{bs} is defined as

$$f_{bs} \triangleq mf_s \tag{2}$$

With the system matrix from the analog architecture, the RMPI reconstructs the multiband signal exploiting a CS algorithm. However, since the matrix is a form of block diagonal, the system matrix is too huge to deal with. For one block, the number of rows and columns respectively corresponds to the number of channels and f_{nyq}/f_s, and the each block is repeated for f_{nyq}/f_{bs} times. The huge block diagonal matrix yields high CC and long reconstructing time, which is impractical for the ES.

In addition, range of the sample sequence containing signal information is Nyquist frequency and it is digitized at interval of $1/T_o$. Hence, for given N signals and the minimum bandwidth $B_{\min}$, the number of non-zero entries in the sequence is more than $2NB_{\min}T_o$. The large number of non-zero entries aggravates success of acquiring the signals.

2.3. The Modulated Wideband Converter (MWC)

To resolve the omission in the RSSR and suggest radar ES system, we exploit the MWC [21], which consists of analog and digital parts. In the analog part, the MWC takes samples that contain compressed information of $x(t)$ at the sub-Nyquist rate. In the digital part, the post DSP and CS recovery algorithm reconstructs the compressed samples as the Nyquist sample of $x(t)$.

In the analog part as shown in Fig.2, the MWC consists of m channels including series of mixer, low-pass filter, and ADC. For each channel, a multiband signal is mixed with the T_p-periodic PR sequence $p_i(t)$. The spectrum of the sequence has $M = 2M_0 + 1$ weighted impulses at intervals of $f_p = T_p^{-1}$. The mixed signal passes an anti-aliasing low-pass filter (LPF) whose cutoff frequency is $f_s / 2 = q f_p / 2$, where $q = 2q_0 + 1 > 0$ is an odd integer. Consequently, from the mixer and LPF, as presented in [21], the input frequency range $[-f_{max} - q_0 f_p, f_{max} + q_0 f_p]$ is divided into $L = 2L_0 + 1$ subbands at intervals of f_p. The subbands are then compressed by multiplying by Fourier coefficients $c_{i,l}$ of the PR sequence and projecting into $[-f_s / 2, f_s / 2)$. Thereafter, the ADC samples the result of the compression at the rate of f_s. For the i-th channel, as presented in [21], the discrete-time Fourier transform (DTFT) of the output of the ADC can be expressed by

$$\breve{y}_i\left(e^{j2\pi f T_s}\right) = \sum_{l=-L_0}^{L_0} c_{i,l} \mathbf{X}(f - l f_p) \tag{3}$$

for $-f_s / 2 \le f < f_s / 2$. The information of $q = f_s / f_p$ subbands are piled in a single row of the $\mathbf{X}$. Note that there are $M \le L$ unique Fourier coefficients of $p_i(t)$ and $q - 1 = L - M$ coefficients are the repetitions. The rest of the process reconstructs the Nyquist sample of $x(t)$ from the compressed samples in the digital part of the MWC.

In the DSP, by disjointing the correlation of the $q - 1$ repeated Fourier coefficients, the *channel expanding method* [21] is applied to extend the number of the equation (3). The channel expanding method is represented by

$$\begin{aligned}
\breve{y}_{i,k}[\hat{n}] &= (y_i[n]e^{-j2\pi k f_p nT_s}) * h_D[n]\Big|_{n=\tilde{n}q} \\
&= (y_i[n]e^{-j2\pi kn/q}) * h_D[n]\Big|_{n=\tilde{n}q}
\end{aligned} \tag{4}$$

where $k \in \{-q_0, \cdots, q_0\}$. As shown in (4), for each k, $y_i[n]$ is modulated with a different frequency kf_p and taken convolutions with q LPFs $h_D[n]$ whose cutoff frequencies are π/q, and then the sequence is decimated by q. As a result, the outcome of channel expanding is

$$\breve{\mathbf{Y}}_i\left(e^{j2\pi fT_p}\right) = \sum_{l=-M_0}^{M_0} c_{i,(l+k)}\mathbf{X}(f - lf_p) \tag{5}$$

for $-f_p/2 \le f \le f_p/2$. Consequently, we can obtain mq equations from the m analog channels. With the continue to finite (CTF) block in [21], the DTFT $\breve{\mathbf{Y}}_i\left(e^{j2\pi fT_p}\right)$ becomes a finite sequence. For the m channels, the equation (5) is expressed as

$$\breve{\mathbf{Y}}[n] = \breve{\mathbf{C}}\breve{\mathbf{Z}}[n] \tag{6}$$

where the measurement matrix $\breve{\mathbf{Y}} \in \mathbb{R}^{mq \times v}$ corresponds to the output of MWC, $\breve{\mathbf{C}} \in \mathbb{C}^{mq \times M}$ is sensing matrix, $\breve{\mathbf{Z}} \in \mathbb{R}^{M \times v}$ contains signal information, v is length of column in $\breve{Y}$ yielded from the CTF block, and $M = 2M_0 + 1$. The matrix equation (6) is exploited to reconstruct the input multiband signal trough a post CS algorithm, and the MWC successfully acquires the signal.
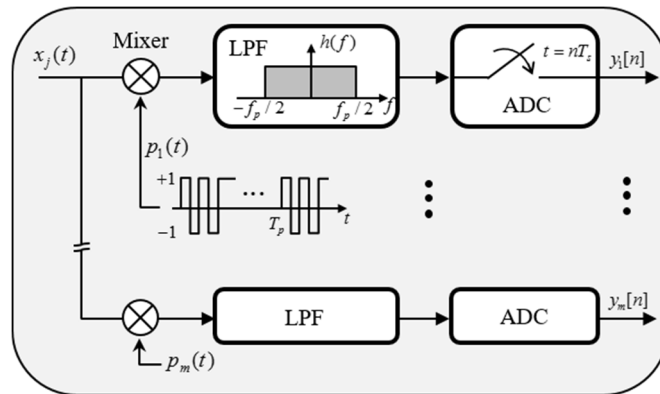
Fig. 4. Analog structure of the MWC [19].

2.3.1. Analysis for the noise folding problem

This section provides an analysis about noise folding effect in the MWC. The MWC consequently divides the Nyquist range into several subbands and gathers into baseband. In this regard, the noise of all the subbands including vacant subbands is also gathered into the baseband, which might result in degradation of signal-to noise ratio (SNR). The degradation of SNR also leads to degradation of reconstruction performance. We verified effect of the noise folding by comparing reconstructed signal between a signal contaminated by colored noise and by white noise. Note that the colored noise is defined as noise only contaminates the actual subband, which contains signal information.

The Fig.5 respectively depicts input signal with white noise and colored noise. Through injecting the two types of signals, we verified reconstructed signals with SNRs, which is defined as

$$SNR = 10 \cdot \log\left(\|x\|_2^2 \,/\, \|n\|_2^2\right) \tag{7}$$

where x and n are respectively the input radar and noise vector. As shown in the Fig. 6, there are noise folding degradation when the SNR is -5dB, while the degradation can be negligible when the signal power is higher than the noise.
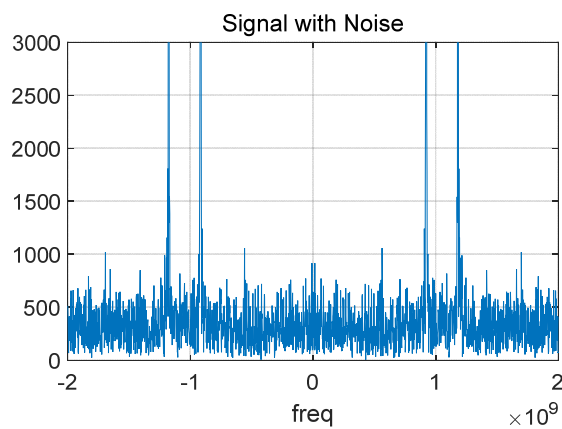
(a)
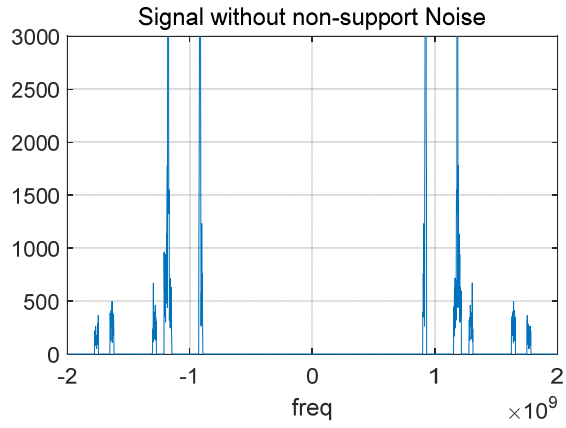
(b)

Fig 5. Input signal with white noise (a), and signal with colored noise (b).
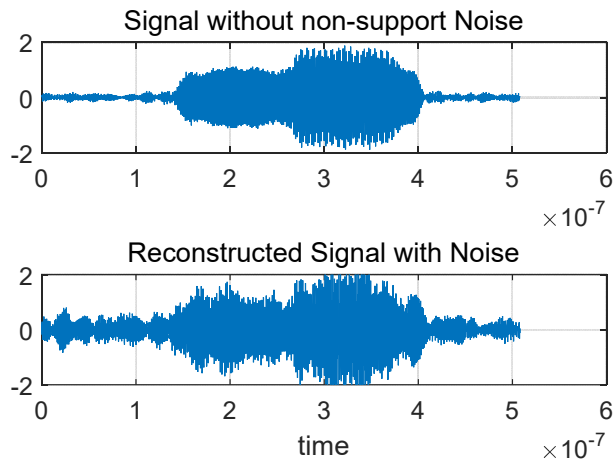
(a)
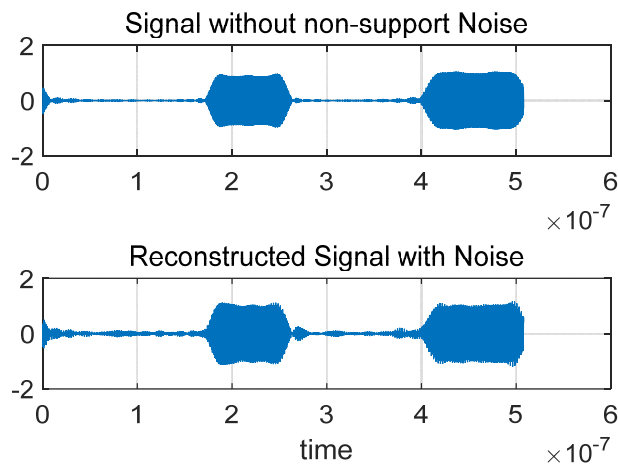
(b)

Fig 6. Original and reconstructed signal with SNR=-5dB (a), and SNR=10dB (b).

III. Signal Acquisition Probability Analysis for the Wideband Signal Receivers

This section is aimed to compare signal acquiring performances of the MWC, RMPI, and RSSR through a noble probability analysis. In case of acquiring a multiband radar signal whose bandwidths are B in a range of f_{nyq}, the analysis can give a guide to design system parameters such as, the number of channels m, sampling rate of ADC f_s, a cycle of PR sequence f_p^{-1}. Instead of implementing all the systems and iterating hundreds of times for varying parameters, the acquisition performances of the receivers can be verified and compared fast and easily.

In the perspective of sampling theorem, successful lossless sub-Nyquist sampling of the MWC for a given sampling rate proportionally depends on the sum of bandwidths of the occupied subbands. Hence, for a given number of input signals, we can expect the success of lossless acquisition once we have the number of occupied subbands. To calculate the probability of successful acquisition, we impose random variables representing the number of input signals, split spectra, and occupied subbands and derive their distributions.

First, we derive a lower bound (LB) of acquisition probability of the MWC. Let X denote the number of received signals in a time slot and Y denote split signals. Then, the conditional probability mass function (PMF) of Y given X can be

$$P_{Y|X}\left(y \mid x\right) = \binom{x}{y}\left(p_s\right)^y\left(1 - p_s\right)^{x-y} \tag{8}$$

where p_s is the probability that a signal is split by the grid of subbands. With assuming that the carrier frequency of the signal is drawn uniformly, we calculate p_s by

$$\begin{aligned}
p_s &= 1 - \sum_{i=-M_0}^{M_0} \int_{if_p - \frac{f_p}{2} + \frac{B}{2}}^{if_p + \frac{f_p}{2} - \frac{B}{2}} \frac{1}{f_{NYQ}}\, dx \\
&= \frac{B}{f_p}
\end{aligned} \tag{9}$$

where $B < f_p$ is the bandwidth of each signal. With a focus on the positive subbands corresponding

realness signals, $K = (R - Y) + 2Y = R + Y$ is the number of occupants (split and un-split spectra). Note that the occupants are not overlapped. The conditional PMF of the occupants K is

$$
\begin{aligned}
P_{K|X}(k \mid x) &= P_{X+Y|X}(x + y \mid x) \\
&\equiv P_{Y|X}(y \mid x) \\
&= P_{Y|X}(k - x \mid x)
\end{aligned}
\tag{10}
$$

The moment generating function (MGF) of the occupants is derived as

$$
\begin{aligned}
M_{K|X}(\mu_x) &= \sum_{k=x}^{2x} e^{\mu_x k} \cdot P_{K|X}(k \mid x) \\
&= \sum_{k=x}^{2x} e^{\mu_x k} \cdot P_{Y|X}(k - x \mid x) \\
&= \sum_{k=x}^{2x} e^{\mu_x k} \cdot {}_x C_{k-x} (p_s)^{k-x} (1 - p_s)^{x-(k-x)}
\end{aligned}
\tag{11}
$$

With assuming that the MWC achieves the lossless sub-Nyquist sampling if and only if $K \leq \kappa_{MWC}$, using the Chernoff bound, the LB of successful sampling is obtained by

$$
\begin{aligned}
P_{MWC}(\text{Successful sampling}) &= P_{K|X}(k \leq \kappa_{MWC} \mid x) \\
&> 1 - \min_{\mu_x \geq 0} e^{-\mu_x \kappa_{MWC}} M_{K|X}(\mu_x)
\end{aligned}
\tag{12}
$$

where the κ_{MWC} is the maximum sparsity such that the CS problem can be perfectly solved. The κ_{MWC} is determined in the equation [21] of

$$
mq \approx 2\kappa_{MWC} \log(M / \kappa_{MWC})
\tag{13}
$$

As presented in [18], the parameters μ_x can be obtained by solving

$$
\mu_x = \arg\min_{\mu_x \geq 0} \left(\ln\left(E[e^{\mu_x x}] \right) - \mu_x \kappa_{MWC} \right)
\tag{14}
$$

By injecting κ_{MWC}, the last of (9) and (11) to the (11), the LB of successful sampling can be denoted by system parameters, such as

$$
\begin{aligned}
&P_{MWC}(\text{Successful sampling}) \\
&> 1 - \min_{\mu_x \geq 0} e^{-\mu_x \kappa_{MWC}} \left(\frac{f_p - B}{\sqrt{B f_p}} \right)^{2x} \sum_{k=x}^{2x} {}_x C_{k-x} \left(\frac{e^{\mu_x} B}{f_p - B} \right)^k
\end{aligned}
\tag{15}
$$

Note that $f_p = f_{nyq} / M$.
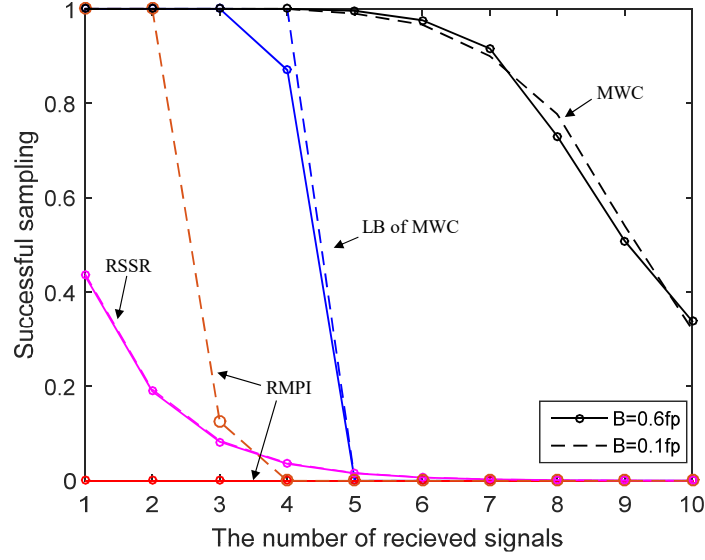
Fig. 7. The probability of signal acquisition among the MWC, RMPI, and RSSR

Second, we derive an acquisition probability of the RMPI. From the architecture of the RMPI, the occupants correspond to digitized signal bands B/T_o^{-1} among digitized Nyquist range f_{nyq}/T_o^{-1}. For the N received signals, the signals occupies at least $N\lfloor BT_o \rfloor$ occupants. Since the band is not always exactly fitted in the digitized graduation, the probability of one more extra occupants is exceeded portion of B compared to the width of the minimum occupants $T_o^{-1}\lfloor BT_o \rfloor$ at one bin T_o^{-1}, i.e.

$$p_{s,RMPI} = \left(B - T_o^{-1}\lfloor BT_o \rfloor\right)/T_o^{-1} = BT_o - \lfloor BT_o \rfloor \tag{16}$$

We then let the maximum recoverable sparsity of RMPI κ_{RMPI} as $m_{RMPI}/2 = f_{nyq}/2f_s$. In the l_0 minimization problem, which is the optimal but mathematically intractable solver, the algorithm can estimate sparsity as half the number of equations [13]. If the RMPI fails to acquire signal with the higher κ_{RMPI} than κ_{MWC}, the MWC demonstrates superiority. Like as (12), the RMPI can be considered to fail the sampling when the minimum occupants $N\lfloor BT_o \rfloor > \kappa_{RMPI}$ and succeed when maximum occupants $N\left(\lfloor BT_o \rfloor + 1\right) < \kappa_{RMPI}$. In the remaining cases, the probability of successful sampling is complement of failure, which is the number of occupant over κ_{RMPI} with $p_{s,RMPI}$. Consequently, the successful sampling probability of RMPI is

$$P_{RMPI}\left(\text{Successful sampling}\right)$$

$$= \begin{cases} 0 & , \quad \lfloor BT_o \rfloor > \kappa_{RMPI} \\ 1 & , \quad N\left(\lfloor BT_o \rfloor + 1\right) < \kappa_{RMPI} \\ 1 - \displaystyle\sum_{i=\lceil \kappa_{RMPI} - N\lfloor BT_o \rfloor \rceil}^{N} p_{s,RMPI}^{i} & , \quad o.w. \end{cases} \qquad (17)$$

Last, we calculate the probability of the RSSR. By noting that only the information of signals whose spectrum is fully located in a band currently being observed by an activated filter bank is preserved in the output samples of the RSSR system, the probability of successful acquisition under an assumption of uniform occurrences of the signals in the frequency domain can be described by

$$P_{RSSR}\left(\text{Successful Sampling}\right) = \left(\frac{W_{BPF} - B}{f_{nyq}/2 - B}\right)^{x} \qquad (18)$$

where W_{BPF} is the bandwidth of the filter banks.

The Fig. 3 depicts that the MWC demonstrated the superiority in terms of the signal acquisition performances. To fairly compare, it was necessary to assign the same number of channels and sampling rate to all the receivers including the RSSR. The MWC and RMPI need at least a $f_s = q f_p$ sampling rate for m channels. In other words, a necessary requirement of the total sampling rate is $mq f_p$. By noting that the RSSR uses a single ADC of the sampling rate W_{BPF}, we can set it to $W_{BPF} = mq f_p$. For the simulation, we set the condition as $m = 4$, $f_{nyq} = 4Ghz$, $f_s = 220Mhz$, $f_p = 31.5Mhz$, $T_o = 1.11\mu s$, and $B = 0.1 f_p$ or $0.6 f_p$. We acquired the empirical result of the MWC exploiting the simultaneous orthogonal matching pursuit (SOMP) [19]. In the simulation the split probability of many signals is lower than theoretical one due to avoid superposition when signal is generated. As shown in Fig. 3, compared to $\kappa_{MWC} = 4$, although we apply the more successful sampling criteria as $\kappa_{RMPI} = 9$ to the RMPI, it could not acquire the signals of $B = 0.6 f_p$. For that signal bandwidth, there was high sparsity, which cannot be recovered by the given SOMP algorithm unlike the MWC. This superiority of the MWC is one reason that we adopt it as the radar ES system. In addition, as shown in (13), we can easily verify the signal acquisition performance through various system parameters, which contributes to design the following radar ES system.

IV. A Radar Electronic Surveillance System Using the MWC

4.1. Problem Formulation

Although the MWC was proposed to acquire a multiband signal, it is difficult to directly implement the MWC for radar ES system. The radar ES meets a problem when the observation time for collecting the compressed samples is retained shorter than the post-processing time consumed for the reconstruction. In this case, continuously incoming signals are stacked and left. Meanwhile, the reconstruction contains complex computations in both of the DSP and CS recovery algorithm. In the DSP, for given v length of sample sequence, CC of the equation (4) is denoted as $O(v^2)$, which is increased rapidly along the enlargement of $v \triangleq T_o / T_s$. To reduce the CC, we can consider enlarging the sampling period T_s of the ADC and/or reducing the observation time T_o to reduce the length v. First, the enlarging sampling period is impractical since it reduces the channel expanding factor q in (4). With the reduced q, the channel expanding method loses the meaning. Second, the reduced observation time cannot be adopted. Since opponent radar system changes their radar signal characteristics, the MWC should observe for a long time to capture them. Meanwhile, we can divide the long observation time into several time slots to reduce CC. However, the dividing scheme occurs another problem, called as time-aliasing [20]. When pieces of a long signal are individually processed and concatenated as the original long signal, there is time-aliasing occurring degradation in reconstruction performance at border of the pieces. When we resolve the time aliasing, we can much reduce CC with similar reconstruction performance.

A number of samples, yielded from the long observation time, requires a high CC in the CS recovery algorithm. The problem of (6) in the MWC is called as multiple measurement vector (MMV) problem, CC of the algorithm is great influenced by the size of measurement matrix. By reducing measurement matrix without miss of signal information, a lower CC can be achieved for the radar ES system
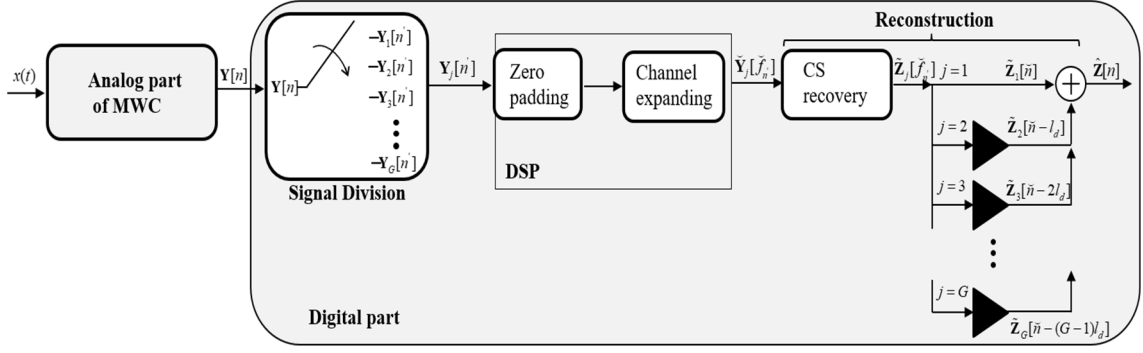
Fig. 8. Block diagram of the radar electronic surveillance system.

4.2. Radar Electronic Surveillance System

The aim of this section is to propose a radar ES system to acquire wideband radar signals. As shown in Fig.4, the radar ES system is designed with the following steps: a *signal division scheme*, a straightforward channel expanding method with zero-padding in the DSP, and signal recovery with a CS algorithm and *integration process* in the reconstruction. To reduce CC in the DSP, we establish the signal division scheme by slicing an observation window as a series of time slots. Second, for a time slot, the relationship between the output of MWC and the sensing matrix of (3) is enlarged with a straightforward channel expanding method in the DSP. In addition, a zero-padding method is presented to alleviate the time aliasing, which is severe when the radar signals exist over the border of time slots. Thereafter, the radar ES system exploits a CS algorithm to recover the signal information. So far, the DSP and signal recovery with a CS algorithm are repeated for every time slots. In the integration process, the recovered signals are integrated with negligible time aliasing. Consequently, the designed system can surveil the radar signals by resolving time aliasing and high CC problem.

4.2.1. Time-slot method

After the analog part of the MWC samples an aggregated radar signals for a long observation time T_o, the radar ES system establishes an uniform grid of the observation time at intervals of time slot T_{sub}. The aggregated radar signals in (1) are redefined as

$$x(t) = \sum_{j=1}^{G} x_j \left(t - (j-1)T_{sub} \right) \tag{19}$$

for $0 \le t < T_{sub}$, where $x_j(t)$ corresponds to the sliced radar signals in the j-th time slot. The number of time slots G is chosen to reduce CC optimally, discussed at the following sub-section. For the j-th time slot, the MWC output (3) can be expressed as

$$\mathbf{Y}_j[n'] = \mathbf{C}\mathbf{Z}_j[n'] \tag{20}$$

where measurement matrix is $\mathbf{Y}_j \in \mathbb{R}^{m \times \tilde{l}_d}$, $\mathbf{C} \in \mathbb{C}^{m \times L}$ is the sensing matrix, $\mathbf{Z}_j \in \mathbb{R}^{L \times \tilde{l}_d}$ contains information of the aggregated radar signal, and

$$\tilde{l}_d = \frac{T_{sub}}{T_s} = q \cdot \frac{T_{sub}}{T_p} = q \cdot l_d \tag{21}$$

The relationship (20) is represented as matrix form by

$$
\begin{pmatrix}
y_{j,1}[1] & \cdots & y_{j,1}\left[\tilde{l}_d\right] \\
\vdots & & \vdots \\
y_{j,m}[1] & \cdots & y_{j,m}\left[\tilde{l}_d\right]
\end{pmatrix}
=
\begin{bmatrix}
c_{1,-L_0} & \cdots & c_{1,0} & \cdots & c_{1,L_0} \\
\vdots & & \vdots & & \vdots \\
c_{m,-L_0} & \cdots & c_{m,0} & \cdots & c_{m,L_0}
\end{bmatrix}
\begin{bmatrix}
z_{j,-L_0}[1] & \cdots & z_{j,-L_0}[\tilde{l}_d] \\
\vdots & & \vdots \\
z_{j,0}[1] & \cdots & z_{j,0}[\tilde{l}_d] \\
\vdots & & \vdots \\
z_{j,L_0}[1] & \cdots & z_{j,L_0}[\tilde{l}_d]
\end{bmatrix}
\tag{22}
$$

The next step is to extent the number m of channels in (20) through a straightforward method.

4.2.2. Digital Channel Expanding Method

We present a straightforward channel expanding method to enlarge the rows of the measurement matrix $\mathbf{Y}_j$ and the sensing matrix $\mathbf{C}$ in (20), and the zero-padding method to alleviate time aliasing. Before expanding the channels, we add qk zeros to the right side of the each row of $\mathbf{Y}_j$ in (22), where $k < l_d$. Thereafter, we exploit that $q = f_s / f_p$ subbands are piled in a single row of the $\mathbf{Z}_j$. In short, by disassembling the q piled subbands, we expand the rows of $\mathbf{Y}_j$ and $\mathbf{C}$ through a Fast Fourier transform (FFT) and simple matrix reorganization. Meanwhile, if there are not zero-paddings

before the FFT, there is severe time aliasing problem since the results from the FFT beyond $\tilde{l}_d$ is lost whereas they should be remained for the next time slot. Thus, we can start with padding zeros, and taking the FFT to the right side of (22) to change the column indices of $\mathbf{Y}_j$ as the frequency axis, i.e., $y_{j,i}[n']$ becomes $y_{j,i}[f_{n'}]$ for $f_{n'} = 1, 2, ..., \tilde{l}_d + qk$.

First, for the i-th row, by disjointing the q piled subbands, we reorganize $\mathbf{Y}_j$ to be a $qm \times (l_d + k)$ matrix such as

$$\breve{y}_{j,i+v}[\breve{f}_{n'}] = \sum_{v=0}^{q-1} y_{j,i}\left[v \cdot (l_d + k) + f_{n'} \right] \tag{23}$$

for $\breve{f}_{n'} = 1, 2, ..., l_d + k$. In the sensing matrix $\mathbf{C}$, by disjointing $q - 1$ repeated $c_{i,l}$ such as $c_{i,M_0+s} = c_{i,-M_0+(s-1)}$ for $s \in [-q_0 + 1, q_0]$, $\mathbf{C}$ is also expanded as

$$\breve{c}_{i+v,l} = \sum_{v=0}^{q-1} c_{i,-L_0+v+l} \tag{24}$$

for $l = 0, 1, ..., M$. Consequently, from the channel expanding methods, the relationship at (20) is transformed as

$$\breve{\mathbf{Y}}_j[\breve{f}_{n'}] = \breve{\mathbf{C}}\breve{\mathbf{Z}}_j[\breve{f}_{n'}] \tag{25}$$

where $\breve{\mathbf{Y}}_j \in \mathbb{R}^{mq \times (l_d+k)}$, $\breve{\mathbf{C}} \in \mathbb{C}^{mq \times M}$, and $\breve{\mathbf{Z}}_j \in \mathbb{R}^{M \times (l_d+k)}$. There is an equal effect of qm enlarged equations which helps to recover the input signals [16]. Meanwhile, the input spectra can occupy up to $4N$ subbands when N real-valued radar signals exist in the time slot because $B_{\max} \leq f_p$ and the conjugate symmetric property $z_{j,l} = z_{j,l}^*$. In other words, since the q piled subbands are disjointed in (25), the input spectra are contained in the $4N$ rows of $\mathbf{Z}_j$.

Compared to the conventional convolution method of (4), CC is reduced by the proposed FFT expanding method. For an one channel, CC of the convolution method is $O(\tilde{l}_d^2)$ whereas the FFT method reduces it as $O(\tilde{l}_d \log \tilde{l}_d)$. In addition, with the signal division scheme, the CC is much reduced as $O\left((\tilde{l}_d + Gk) \log(\tilde{l}_d / G + k)\right)$. Since the ES system samples the radar signals for a long time, the

effect of additional k zeros are negligible, $k \ll \tilde{l}_d$. The number of time slot G can be considered as

$$G = \arg\min_{G \in \mathbb{N}} \left(\tilde{l}_d + Gk \right) \log \left(\tilde{l}_d / G + k \right) \tag{26}$$

For instance, when $l_d = 256$, $k = 2$, $G = 76$, CCs of each of convolution expanding method, FFT method, and FFT method with signal division scheme are respectively *65536*, *2048*, and *685*. The reduced CC of the last contributes to achieve fast computing

4.2.3. Synthetization and Reconstruction

A CS algorithm recovers the signal information as $\tilde{\mathbf{Z}}_j[\breve{f}_n] \in \mathbb{R}^{4N \cdot (l_d + k)}$ by solving the MMV problem of (25), and the $\tilde{\mathbf{Z}}_j[\breve{n}]$ is generated by taking IFFT. The procedures from the DSP to generation of $\tilde{\mathbf{Z}}_j[\breve{n}]$ are repeated for G time slots, and the results from every time slots are integrated as

$$\hat{\mathbf{Z}}[n] = \sum_{j=1}^{G-1} \tilde{\mathbf{Z}}_j[\breve{n} - (j-1)l_d] + \tilde{\mathbf{Z}}_G[\breve{n} - (G-1)l_d] \tag{27}$$

where the matrix $\tilde{\mathbf{Z}}_G$ of last time slot decimates columns in $[l_d + 1, \ l_d + k]$. As depicted in Fig. 4, the each $\tilde{\mathbf{Z}}_j$ are delayed for l_d using buffers and integrated such as the $[l_d + 1, \ l_d + k]$ columns of $\tilde{\mathbf{Z}}_{j-1}$ are added to front k columns of $\tilde{\mathbf{Z}}_j$. With zero-padding in the DSP and the integration process, we alleviate the time aliasing yielded from the radar signals being located at the border of time slots and show the improvement in section VI. The time-wise information including the PRI, TOA, and TOD can be found through the reconstructed radar waveform or the estimation method presented in [17]. The carrier frequencies can be estimated by exploiting pulse spectrum density (PSD) estimation [18].

The parameters of the proposed system are arranged in Table I. For a given analog system, PR sequence parameters, sampling rate of ADC, and the number of channels are the dependent parameters. While a long observation time   is adopted to capture radar signals, it rapidly increases CC in DSP

unit. Note that the long observation time also improves frequency resolution. However, the signal division scheme and the straightforward DSP method contributed to reduce the reconstructing time. Furthermore, the reconstructing time can be more reduced with a preprocessing method discussed at the next section.

TABLE I. Parameters of the radar ES system

Parameters (Symbol)	Relationship	Value
Observation time (T_o)	$T_o = G \cdot T_{sub}$	$0.1302\ ms$
The number of time slots (G)	-	100
Nyquist frequency (f_{nyq})	$f_{nyq} \geq f_{max}$	$4\ GHz$
Bandwidth (B)	$B_{min} \leq B \leq B_n$	$\leq 31.49\ MHz$
◊ Channel expanding factor (q)	> 0	7
◊ Period of PR sequences (T_p)	$T_p = 1/f_p$	$0.03176\ ns$
◊ Sampling rate of ADC (f_s)	$f_s = q \cdot f_p$	$220\ MHz$
◊ The number of PR pattern (M)	$M = L - q + 1$	127
◊ Physical channels (m)	-	4
◊ Virtual channels ($\breve{m}$)	$\breve{m} = mq$	28

The dependent parameters are denoted as ◊ for a given hardware.

4.3. Preprocessing of MMV algorithm

This section aims to propose a *sub-sampling* method, which is a preprocessing to proportionally reduce CC of the following MMV recovery algorithm. As discussed at the previous section, the radar ES system could greatly reduce CC of the DSP by dividing the long observation time into time-slots. However, since the total CC of MMV recovery of (25) is still high due to the long observation time, the reconstructing time can exceed the observation time. As presented at (26), note that the long observation time enlarges the total number of measurement vectors as Gl_d. Since MMV recovery algorithm contains matrix multiplication and/or inversions, CC of the algorithm is rapidly increased along the number of measurement vectors. Thus, we propose the sub-sampling method, which is a preliminary work to reduce CC of the following MMV algorithm. This method strategically selects some measurement vectors without missing the support set. The support set indicates indices of nonzero sub-bands. The sub-sampling method is presented at the sub-Section A, and the benefit of CC and support recovery performance are presented at the sub-Section B.

4.3.1. Sub-Sampling Method

By the linearity at (25), choosing columns of $\breve{\mathbf{Y}}_j$ is equivalent to choosing columns of the signal matrix $\breve{\mathbf{Z}}_j$. We therefore choose the columns of $\breve{\mathbf{Y}}_j$ based on the structure of the signal matrix $\breve{\mathbf{Z}}_j$. The rows of $\breve{\mathbf{Z}}_j$ contain spectrally orthogonal subbands of the discrete spectrum of $x(t)$ at the intervals of f_p. By the discrete Fourier transform, the column indices represents a frequency grid of intervals of $1/T_{sub}$. In the rows, every narrow band spectrum of $x_j(t)$ is contained. Some of the narrow band spectra may be split by the borderline of the subbands based on their center frequencies.

In this scenario, we propose a sub-sampling method depicted at Fig.5. This method generates subsets
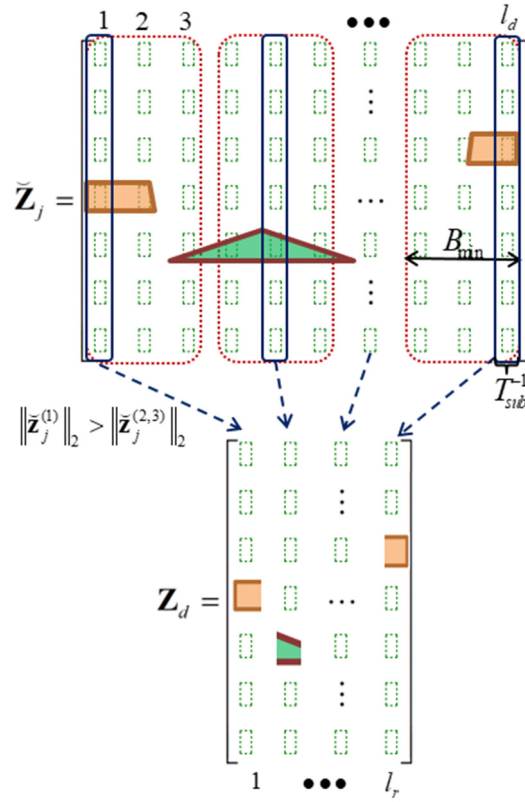
Fig. 9. Selected columns of measurement matrix contain essential signal information to detect a support set while reducing computational burden.

by classifying columns of $\breve{\mathbf{Y}}_j$ at intervals less than minimum signal bandwidth $B_{\min}$. For each subset, the method selects one column having a maximum energy. When the subset consists of columns less than $B_{\min}$, the method can avoid the worst situation that several signals exist in a subset and are not overlapped in the column axis. For that situation, one of the signals is selected and the others are omitted. On the other hand, a sub-sampled matrix $\mathbf{Y}_d \in \mathbb{R}^{mq \times l_r}$, union of selected columns, contains components of all the signal while reducing the size of measurement matrix. The number of sub-sampled column is calculated as

$$l_r = \left\lceil l_d / \left\lfloor B_{\min} T_{sub} \right\rfloor \right\rceil \tag{28}$$

where $\left\lfloor B_{\min} T_{sub} \right\rfloor$ is the element number of the subset. The notation $\breve{\mathbf{Z}}_j$ also becomes $\mathbf{Z}_d \in \mathbb{R}^{M \times l_r}$. Since this simple sub-sampling method works at once before the following iterative MMV recovery algorithm, CC yielded from sub-sampling method can be negligible. The reduced column l_r proportionally reduces CC in the following MMV recovery algorithm, and we pick the SOMP [19] to

verify the CC benefit and the support recovery performance.

4.3.2. Performance Analysis of the Algorithm

To verify CC benefit of sub-sampling method, we adopt SOMP [19], which is a solver for the MMV problems. The SOMP is an iterative algorithm, where at each iteration the SOMP recovers an index of nonzero rows of a signal matrix $\mathbf{Z}_d$, i.e. supports set, in (25) by matching a MMV matrix $\mathbf{Y}_d$ with bases of the sensing matrix $\breve{\mathbf{C}}$.

The procedure of SOMP is adjust for the radar ES system to enhance the algorithm efficiency and reduce CC. The terminal condition is

$$\left\| \mathbf{Y}_d \right\|_2 \leq EPS. \tag{29}$$

Unless the condition is satisfied, the algorithm continues to estimate a support among a set Λ defined as row indices of $\mathbf{Z}_d$, which is

$$J = \arg\max_{\Lambda} \left\| \mathbf{C}_\Lambda{}^H \mathbf{Y}_{residue}[i] \right\|_2 \tag{30}$$

where $\mathbf{C}_\Lambda$ is a column of $\breve{\mathbf{C}}$ and i is iteration index. At first iteration, $\mathbf{Y}_d$ replaces the $\mathbf{Y}_{residue}$. From the conjugate symmetric property of real-valued radar signal, the selected and symmetric supports are stored in the S_i, and S_i are gathered at S, i.e. $S = \{S_i | i = 1, 2, ..., N\}$. After estimating the support set S containing $2i$ elements, the residual of $\mathbf{Y}_d$ is generated by

$$\mathbf{Y}_{residue} = \mathbf{Y}_d - \mathbf{C}_S \cdot \mathbf{C}_S^\dagger \mathbf{Y}_d \tag{31}$$

Note that N real-valued radar signals can yields up to $4N$ supports. The SOMP detects the support set Ω for upmost $2N$ iterations. The signal information is reconstructed as

$$\tilde{\mathbf{Z}}_j[\breve{f}_n] = \mathbf{C}_\Omega^\dagger \cdot \breve{\mathbf{Y}}_j[\breve{f}_n] \tag{32}$$

where $\mathbf{C}_\Omega^\dagger$ is a Moore-Penrose pseudoinverse of outcome by extracting the columns of Ω from $\breve{\mathbf{C}}$ in (25). The result of (32) can be used for the integration process explained at the Section IV-C.
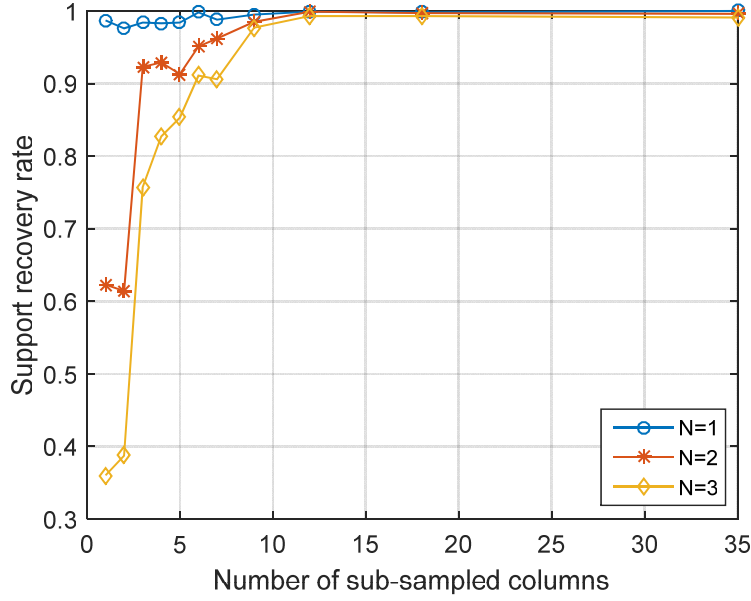
Fig. 10. Support recovery rate along the number of sub-sampled column of measurement matrix in the SOMP.

To verify CCs, we focus on the matrix multiplication and inverse parts (30) and (31) in the algorithm, which are main factors enlarging CC. For an observation time, the sizes of measurement and sensing matrix are respectively $\breve{m} \times l_d$ and $\breve{m} \times M$, where $\breve{m} = mq$. In the equation (30), CC is $O(M\breve{m}l_d)$. In the equation (31), although the CCs are different for the each i-th iteration due to $\mathbf{C}_S \in \mathbb{C}^{\breve{m} \times 2i}$, but we ignore the i to verify easily, where $i < \breve{m}$. Thus, the CC of (31) becomes $O(\breve{m}^2(l_d + 2) + 16\breve{m})$. As a result, the total complexity for N signals becomes

$$O\left(2N\left(l_d\breve{m}\left(M + \breve{m} + 2\right) + 16\breve{m}\right)\right) \tag{33}$$

Second, we compute CC with SS method. The CC becomes

$$O\left(2N\left(l_r\breve{m}\left(M + \breve{m} + 2\right) + 16\breve{m}\right)\right) \tag{34}$$

where $l_r < l_d$ is the number of sub-sampled columns. In the result of (34), CC is reduced proportionally with the small l_r.

The Fig.6 depicts the support recovery rate along the number of sub-sampled columns of the measurement matrix. The support recovery rate is defined: when the recovered support set is a subset of the original, the flag is one. We verified the support recovery rate along the number of subsets
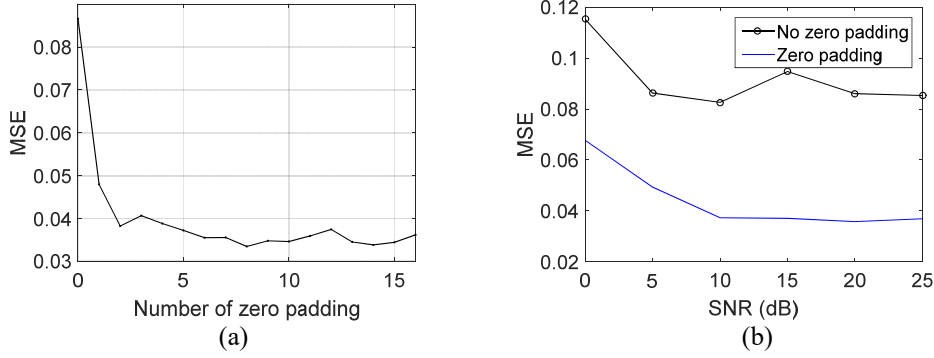
Fig. 11. The zero padding method improves the reconstruction performance, and two zeros are used in the (b)

corresponding to number of sub-sampled column compared to the original columns $l_d = 35$. The minimum bandwidth of a signal was $B_{\min} = 0.1 f_p = 3.15 MHz$. From the (28), the calculated l_r is *12*, which has similar recovery performance to full columns. This implies that the sub-sampled MMV $\mathbf{Y}_d$ does not miss the signal information and includes all the essential parts of the original MMV $\breve{\mathbf{Y}}_j$. In this scenario, the sub-sampling method can proportionally reduce CC as *1/3*. Consequently, the sub-sampling method proportionally reduces CC while keeping similar recovery performance.

4.4. Simulation Result

Through simulations, we verified that the radar ES acquires a multiband signal by alleviating the time aliasing. For the simulations, we generated 3 pulsed radar signals whose carrier frequencies existed randomly from $f_{\min} = 0.5 GHz$ to $f_{\max} = 2 GHz$. We inputted 5dB signals when SNR is not discussed. The signal to noise ratio (SNR) is defined as $10 \cdot \log\left(\|x\|_2^2 / \|n\|_2^2\right)$, where x and n are respectively the input radar and noise vector. We considered a 4-channel MWC system, and the remained system parameters were shown at Table I. We set the number of time slots as $G = 100$ time slots. To recover the multiband signal, we used the SOMP with SS method discussed at the previous section V.

We first verified the improvement of time aliasing in the sense of mean square error (MSE) by using
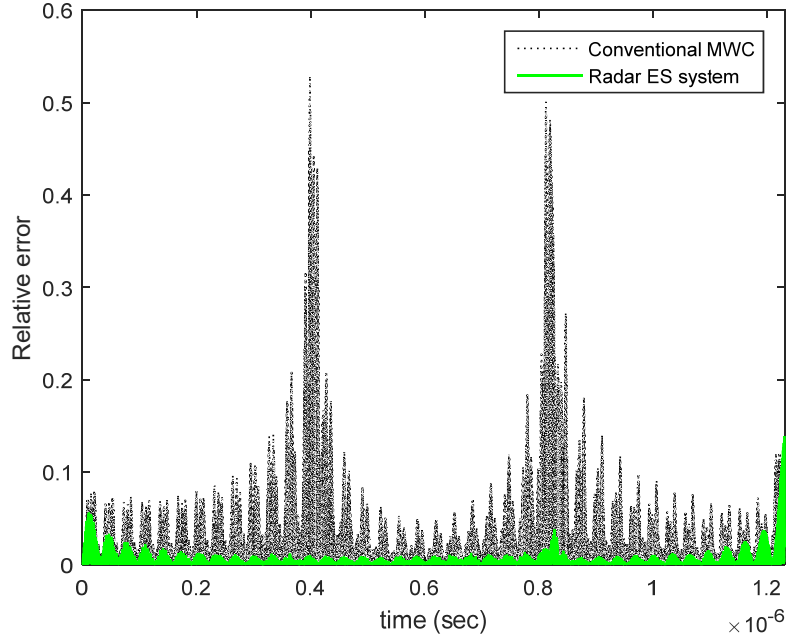
Fig. 12. The relative errors among the timeslots are alleviated with the radar ES system.

the zero-padding method and integration process. The MSE is defined as $\|x - x_r\|_2^2 / \|x\|_2^2$, where x and

x_r are respectively original and the recovered radar vector. As shown in Fig. 6a, the reconstruction

error was improved along the number of zeros. Although the number of zero yields the additional

number k of columns in the channel expanded measurement matrix, compared to the original column

number $l_d = 35$, the result showed that small number of zeros even show the benefit. As shown in Fig.

6b, with $k = 2$ zeros, the MSEs were improved evidently. Last, by setting a shorten observation period

$GT_{sub} = 1.29 \mu s$, we clearly verified the improvement of time aliasing among the border of time slots.

In this simulation, the relative error was defined as

$$relative\_error[i] := \|x[i] - x_r[i]\|_2^2 \qquad (35)$$

where $x[i]$ is input radar value at the i-th time. As shown in Fig. 7, compared to just affixing time

slot, the errors among the time slots are improved evidently, which means the radar ES system can

acquire radar signals with similar reconstruction performance.

IV. Calibration methods for the MWC

5.1. Problem Formulation

The MWC can reconstruct the Nyquist sample $x[\tilde{n}]$ from the compressed samples $y_i[n]$ by using the theoretical model of (39) when every analog component is ideally designed. However, the transfer matrix $\mathbf{C}$ of (40) does not contain the practical analog characteristics including failure of clock synchronization between the PR sequence and the ADC, irregular channel gains, and the non-ideal responses of the LPF. Since the model mismatch by the non-ideal responses of the LPF can be easily eliminated by digital equalizing filters [17], we focus on the other non-idealities ensuring the linearity in (39) and the calibration using single tones with unknown phase information..

The non-idealities are usually posed when the MWC is implemented. For examples, there are asynchronization between the PR sequence and the ADC and irregularity among channel gains. In theory, the transfer model of (40) assumes perfect synchronization between the initial starting points of the PR sequence and the ADC. However, the synchronization requires additional circuits, and unknown path delays on the channels may disturb the synchronization. We model the asynchronization as a time difference of the initial points between the ADC and the PR sequence, which is equivalent to giving an unknown delay τ_i to $p_i(t)$ in Fig. 1. Likewise, for the irregular channel gains, we give an unknown channel gain w_i to $p_i(t)$. By the definition, the elements of the transfer matrix $\breve{\mathbf{C}}$ distorted by the asynchronization and the irregular channel gains are derived as

$$
\begin{aligned}
\breve{c}_{i,l} &= \frac{1}{T_p} \int_{\tau_i}^{T_p + \tau_i} w_i \cdot p_i(t - \tau_i) e^{-j 2\pi f_p l t} \cdot dt \\
&= w_i e^{-j 2\pi f_p l \tau_i} \frac{1}{T_p} \int_0^{T_p} p_i(t) e^{-j 2\pi f_p l t} \cdot dt \\
&= w_i e^{-j 2\pi f_p l \tau_i} \cdot c_{i,l}
\end{aligned}
\tag{36}
$$

The asynchronization and irregularity among channel gains respectively multiplies complex

exponentials and magnitudes to every column and row of (4). Consequently, some non-idealities of analog components distort the transfer matrix $\mathbf{C}$ while keeping the linearity.

By noting that the columns of unknown $\mathbf{\breve{C}}$ correspond to frequency response of the sampling system, we can estimate every frequency response by sequentially injecting single tone signals owing to the linearity of the distorted system. However, when the phases of the input single tone signals are unknown, which results in another complex exponentials in outputs, the estimated response is still untrustworthy. Such a case is impractical since the unknown path delays in analog channels make it hard to predict the phase of outputs even if the phase of input tone is elaborately controlled. Thus, it is needed to develop a calibration algorithm using tone signals with unknown phases for a practical implementation of the MWC

5.2. Calibration with DC signals

Before proposing a calibration method, some details about the MWC regarding calibration is summarized. By representing $p_i(t)$ as a form of the Fourier series expansion of bases $e^{-j2\pi f_p lt}$ for $l = -\infty, \cdots, \infty$, the output of i-th channel $y_i[n]$ is represented as

$$
\begin{aligned}
y_i[n] &= \sum_{l=-\infty}^{\infty} c_{i,l} \cdot LPF\{x(t) \cdot e^{-j2\pi f_p lt}\}\Big|_{t=nT_s} \\
&= \sum_{l=-L_0}^{L_0} c_{i,l} \cdot LPF\{x(t) \cdot e^{-j2\pi f_p lt}\}\Big|_{t=nT_s}
\end{aligned}
\tag{37}
$$

where $LPF\{\cdot\}$ is the low-pass filtering operator, and the infinite order of summation is reduced to a finite order of $L = 2L_0 + 1$ since $x(t)$ is bandlimited and the bandwidth of LPF out of the maximum frequency outputs zero. Note that the reduced order is calculated by $L_0 = M_0 + q_0$ [6]. Fourier series coefficients $c_{i,l}$ of $p_i(t)$ is defined by

$$
c_{i,l} \triangleq \frac{1}{T_p} \int_0^{T_p} p_i(t) e^{j\frac{2\pi}{T_p} lt}
\tag{38}
$$

For an observation time T_o, the matrix form of (37) is

$$
\mathbf{Y} = \mathbf{CZ}
\tag{39}
$$

where $y_i[n]$ and $LPF\{x(t) e^{-j2\pi f_p lt}\}\Big|_{t=nT_s}$ respectively exist in the i-th row of $\mathbf{Y} \in \mathbb{R}^{m \times l_d}$ and the l-th row of $\mathbf{Z} \in \mathbb{C}^{L \times l_d}$ for $n = 0, \cdots, l_d - 1$, and $l_d = T_o / T_s$. The transfer matrix $\mathbf{C} \in \mathbb{C}^{m \times L}$ is

$$
\mathbf{C} = \begin{bmatrix} c_{1,-L_0} & \cdots & c_{1,0} & \cdots & c_{1,L_0} \\ \vdots & & \vdots & & \vdots \\ c_{m,-L_0} & \cdots & c_{m,0} & \cdots & c_{m,L_0} \end{bmatrix}
\tag{40}
$$

where $c_{i,-l} = c_{i,l}^*$ and $(*)$ is a complex conjugate operator. Thereafter, additional digital signal

processing (DSP) and a CS recovery algorithm reconstruct the Nyquist sample $x[\tilde{n}]$ of the input $x(t)$.

5.2.1. Calibration Algorithm

We provide a calibration algorithm using single tone signals with unknown phase information for estimation of linear system transfer of the MWC. In specific, we suppose that the system is distorted while keeping the linearity, and our goal is to calibrate a distorted system transfer $\tilde{\mathbf{C}}$. The calibration algorithm consists of two steps; *linear estimation* and *phase equalization*. In the linear estimation step, we input sinusoids with unknown phases to the distorted MWC. Based on a mathematical relationship between the input tone signals and the output samples, we estimate the frequency responses of the system transfer. However, due to the unknown phases of the tone signals, the estimate still contains uncertain components. In the phase equalization step, we equalize the effect of the unknown phases by exploiting a structural characteristic in a matrix representation of the input-output relationship. The phase equalization step outputs the distorted system transfer of a single analog channel of the MWC.

In the linear estimation step, for the i-th channel, we sequentially input tone signals of

$$s(t) = e^{j2\pi f_p k(t-\tau_{i,k})} \tag{41}$$

for $k = 0,1,\cdots,M_0$, where $\tau_{i,k}$ are the priorly unknown phases, which are different among input frequencies and channels. From (37), the output $\tilde{y}_{i,k}[n]$ is derived as

$$
\begin{aligned}
\tilde{y}_{i,k}[n] &= \sum_{l=-L_0}^{L_0} \tilde{c}_{i,l} \cdot LPF\{e^{j2\pi f_p k(t-\tau_{i,k})} \cdot e^{-j2\pi f_p l t}\}\Big|_{t=nT_s} \\
&= \sum_{l=-L_0}^{L_0} \tilde{c}_{i,l} \cdot \theta_{i,k}^k \cdot LPF\{e^{-j2\pi f_p (l-k)t}\}\Big|_{t=nT_s}
\end{aligned}
\tag{42}
$$

where $\tilde{c}_{i,l}$ is elements of the distorted transfer matrix $\tilde{\mathbf{C}}$ and

is represented as effects of unknown phases. The frequencies $f_p(l-k)$ within the bandwidth of LPF

f_s is remained in (42), and the order of summation L_0 is reduced to q_0 when

$$|l-k| \le q/2 \tag{43}$$

The inequality (43) is yielded from $\left|f_p(l-k)\right| \le f_s/2$ and $f_s = qf_p$. From (43), the last of (42) is

derived as

$$\tilde{y}_{i,k}[n] = \sum_{l=-L_0}^{L_0} \tilde{c}_{i,l} \cdot \theta_{i,k}^k \cdot e^{-j2\pi f_p(l-k)t}\Bigg|_{t=nT_s}, \quad |l-k| \le \frac{q}{2}$$

$$= \sum_{l=-q_0}^{q_0} \tilde{c}_{i,l+k} \cdot \theta_{i,k}^k \cdot e^{-j2\pi l\frac{n}{q}} \tag{44}$$

For $k = 0, 1, \cdots, M_0$, the last equation of (44) can be represented as a matrix form of

$$\tilde{\mathbf{Y}}_i = \mathbf{P}_i \tilde{\mathbf{A}}_i \mathbf{F}^{\mathbf{H}} \tag{45}$$

where $\tilde{\mathbf{Y}}_i \in \mathbb{R}^{(M_0+1)\times l_d}$, $\mathbf{P}_i \in \mathbb{C}^{(M_0+1)\times(M_0+1)}$, $\tilde{\mathbf{A}}_i \in \mathbb{C}^{(M_0+1)\times q}$, and $\mathbf{F}^{\mathbf{H}} \in \mathbb{C}^{q\times l_d}$ are readily represented as,

$$\underbrace{\begin{bmatrix} \tilde{y}_{i,k=0}[0] & \cdots & \tilde{y}_{i,k=0}[l_d-1] \\ \vdots & & \vdots \\ \tilde{y}_{i,k=M_0}[0] & \cdots & \tilde{y}_{i,k=M_0}[l_d-1] \end{bmatrix}}_{\tilde{\mathbf{Y}}_i} =$$

$$\underbrace{\begin{bmatrix} \theta_{i,0}^0 & & \\ & \ddots & \\ & & \theta_{i,M_0}^{M_0} \end{bmatrix}}_{\mathbf{P}_i} \underbrace{\begin{bmatrix} \tilde{c}_{i,-q_0} & \cdots & \tilde{c}_{i,q_0} \\ \vdots & & \vdots \\ \tilde{c}_{i,-q_0+M_0} & \cdots & \tilde{c}_{i,q_0+M_0} \end{bmatrix}}_{\tilde{\mathbf{A}}_i} \underbrace{\begin{bmatrix} e^{-j2\pi(-q_0/q)\cdot 0} & \cdots & e^{-j2\pi(-q_0/q)\cdot(l_d-1)} \\ \vdots & & \vdots \\ e^{-j2\pi(q_0/q)\cdot 0} & \cdots & e^{-j2\pi(q_0/q)\cdot(l_d-1)} \end{bmatrix}}_{\mathbf{F}^H}$$

$$(46)$$

The matrices $\tilde{\mathbf{Y}}_i$ and $\mathbf{F}^{\mathbf{H}}$ are already known, but $\mathbf{P}_i$ and $\tilde{\mathbf{A}}_i$ are unknown. Meanwhile, $\tilde{\mathbf{A}}_i$

contains elements of distorted system transfer $\tilde{\mathbf{C}}$. Note that our aim is estimation of distorted system

transfer. The matrix $\mathbf{F^H}$ is a form of discrete Fourier transform (DFT) matrix and become full rank matrix when $l_d \geq q$. This condition can be achieved by injecting the signals for an observing time $T_o \geq qT_s$ since $l_d = T_o / T_s$. By multiplying Moore-Penrose pseudoinverse $\mathbf{F}^\dagger$ of $\mathbf{F^H}$ to the right side of (45), it turns into

$$\tilde{\mathbf{Y}}_i \mathbf{F}^\dagger = \widehat{\mathbf{P}_i \tilde{\mathbf{A}}_i} \tag{47}$$

We define $\mathbf{B}_i \triangleq \tilde{\mathbf{Y}}_i \mathbf{F}^\dagger$ whose the (k,l)-th element equals to

$$
\begin{aligned}
b_{k,l} &= \left(\widehat{\mathbf{P}_i \tilde{\mathbf{A}}_i} \right)_{k,l} \\
&= \theta_{i,k-1}^{k-1} \cdot \tilde{c}_{i,-q_0+(k+l-2)}
\end{aligned}
\tag{48}
$$

As shown in the result of linear estimation (48), the elements $\tilde{c}_{i,l}$ of distorted transfer matrix are multiplied with elements of $\mathbf{P}_i$. Thus, to acquire the elements $\tilde{c}_{i,l}$ from $\tilde{\mathbf{A}}_i$, we should estimate or equalize the $\mathbf{P}_i$.

In the phase equalization step, we exploit that $\tilde{\mathbf{A}}_i$ is a Hankel matrix, i.e. $(k+1,l-1)$ element equals to (k,l) element for $k \geq 1$, $l > 1$. We generate a matrix $\mathbf{G}_i = diag\{g_1, g_2, ..., g_{M_0+1}\}$ to equalize the unknown phase matrix $\mathbf{P}_i$. All the elements of $\mathbf{G}_i$ are defined as

$$
g_k \triangleq \begin{cases} 1 & , \ k = 1 \\ g_{k-1} \cdot \dfrac{b_{k-1,2}}{b_{k,1}} & , \ otherwise \end{cases}
\tag{49}
$$

By the definition of (48), the elements g_k are equal to the inverse of the k-th elements of $\mathbf{P}_i$. In specific,

$$
\begin{aligned}
g_k &= g_1 \prod_{j=1}^{k-1} \frac{b_{j,2}}{b_{j+1,1}} \\
&= g_1 \prod_{j=1}^{k-1} \frac{\theta_{i,j-1}^{j-1} \cdot \tilde{c}_{i,-q_0+j}}{\theta_{i,j}^{j} \cdot \tilde{c}_{i,-q_0+j}} \\
&= g_1 \cdot \frac{\theta_{i,0}^{0} \prod_{j=2}^{k-1} \theta_{i,j-1}^{j-1}}{\theta_{i,k-1}^{k-1} \prod_{j=1}^{k-2} \theta_{i,j}^{j}} \\
&= \left(\theta_{i,k-1}^{k-1} \right)^{-1}
\end{aligned}
\tag{50}
$$

Hence, the multiplication $\mathbf{G}_i \widehat{\mathbf{P}}_i$ becomes identity matrix $\mathbf{I}$. Consequently, we can estimate the $\tilde{\mathbf{A}}_i$

by multiplying $\mathbf{G}_i$ to (48), i.e.

$$
\widehat{\tilde{\mathbf{A}}_i} = \mathbf{G}_i \mathbf{B}
\tag{51}
$$

The result of equalization $\widehat{\tilde{\mathbf{A}}_i}$ contains positive frequency elements $\tilde{c}_{i,l}$ for $l = 0,1,...,L_0$. The

negative elements are acquired by using the conjugate symmetric property of transfer matrix $\tilde{c}_{i,-l} = \tilde{c}_{i,l}^{*}$.

Thus, by injecting calibration signals to the i -th channel of MWC, we can estimate i -th row of

distorted transfer matrix $\tilde{\mathbf{C}}$. For the m channels, the linear estimation and phase equalization are

repeated. The calibrated transfer matrix $\tilde{\mathbf{C}}$ is acquired from the m estimated rows. With the

calibrated transfer matrix $\tilde{\mathbf{C}}$, the unknown multiband signal can be reconstructed successfully.

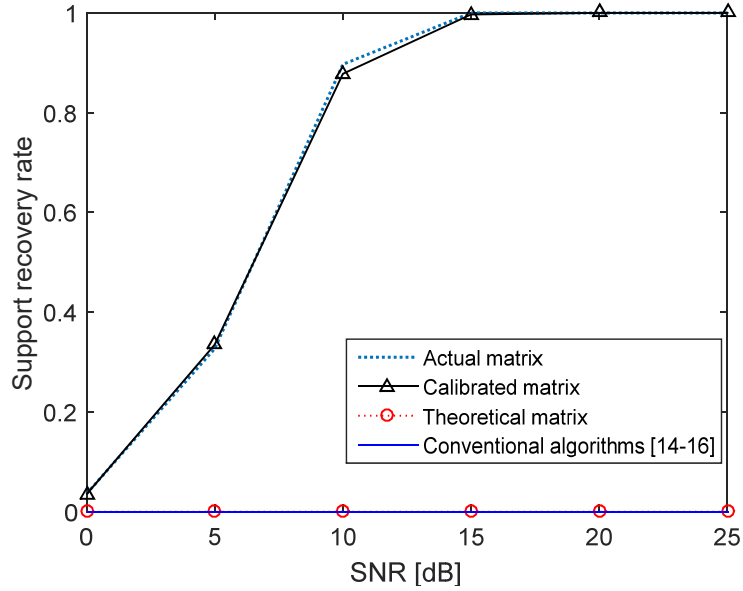## 5.2.2. Simulation

Fig. 13. Support recovery rates under various SNRs of unknown input signals. The system transfer matrix calibrated by the proposed algorithm and the theoretical matrix ignoring practical conditions are used.
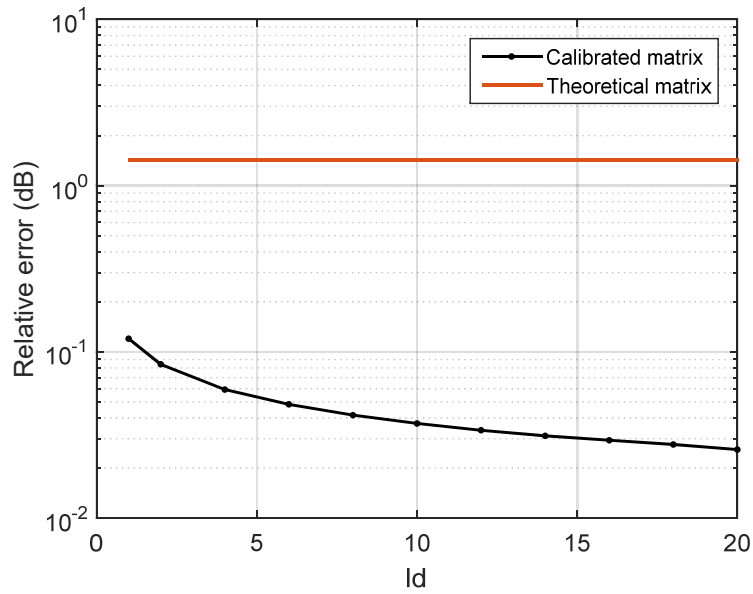

Fig. 14. Relative errors of the calibrated and theoretical matrix compared to the actual system transfer. The parameter l_d means time of injecting calibration signals.

In this section, the simulations were presented to verify the performance of proposed calibration algorithm. For the simulation, we generated an unknown multiband signal $x(t)$, which consisted of 6 disjoint bands with $f_{\max} = 2GHz$. We used 4-channel MWC to sample $x(t)$. There were $M = 127$ Fourier coefficients of PR sequence at intervals of $f_p = 31.5MHz$, and the sampling rate of ADC was $f_s \simeq 220MHz$, which induced $q = 7$. To construct a distorted environment, we set an asynchronization as a certain time difference of the initial points between the ADC and the PR sequence to $7 \cdot T_p$. To estimate the distorted transfer matrix $\tilde{\mathbf{C}}$, we injected $30dB$ tones as (41). The signal-to noise ratio (SNR) was defined as $SNR = 10 \cdot \log_{10}(\|s\|_2^2 / \|n\|_2^2)$, where s and n were respectively the calibration signal and noise vector. In addition, we also generated unknown input phases $\tau_{i,k} \in [0, T_o]$ randomly. We exploited the SOMP [19] to estimate supports of x from the compressed outputs $y_i[n]$. Note that the supports correspond to actual indices of signal spectra among subbands.

We compared the recovery performances using the calibrated transfer matrix and theoretical transfer matrix without calibration. We also generated the actual transfer matrix $\mathbf{C}_a$ from the distorted environment. To verify success of recovery, we measured the supports recovery rate whose flag is denoted as one when the recovered supports were coincided to original supports. As shown in Fig.2, the theoretical transfer matrix failed to recover the original supports due to the distortion by the asynchronization between the ADC and the PR sequence. On the contrary, the calibrated transfer matrix successfully recovered them like the actual matrix. In addition, to verify the importance of the phase equalization step in calibration, we implemented the conventional calibration algorithms of [14]–[17]. The proposed phase equalizing calibration only succeeded to recover the supports when the unknown input phases exist. The algorithms of [15], [16] cannot cover the distortion of asynchronization. Above all, since the system transfer is distorted by the remained unknown phases again, their failures were unavoidable. Hence, the phase equalization should be executed for the successful calibration.

We demonstrated the effects of the increased injecting time of calibration signals. By increasing the injecting time, the number of compressed samples l_d of (45) was enlarged, which contributed to

estimate the actual transfer matrix more precisely. To verify it, we compared relative errors of the calibrated and theoretical matrix to the actual matrix $\mathbf{C}_a$ along the l_d. The relative error was defined as

$$Relative\ \ error = \left\| \tilde{\mathbf{C}} - \mathbf{C}_a \right\|_F / \left\| \mathbf{C}_a \right\|_F \tag{52}$$

where $\tilde{\mathbf{C}}$ is calibrated or theoretical matrix, and $\left\| \cdot \right\|_F$ is Frobenius norm. As shown in Fig. 3, the calibrated sensing matrix was closed to the actual matrix unlike the theoretical matrix. The relative errors of theoretical matrix were a certain constant, because the asynchronization and the system transfer are unchanged. Consequently, the result demonstrated that calibration performance was enhanced along the l_d.

5.3. Calibration without DC signal

Although the calibration method discussed at the previous section is intuitive and straightforward method, it is important to using DC signal to estimate initial information, while the remained estimation procedures are cascade. If the MWC restricts the frequency scope as $f_{min} \sim f_{max}$, the DC signal is blocked and the calibration with DC method is invalid no more. In this scenario, cosine tones with an off-set frequency are injected in descending order such as, $k = M_0, M_0 - 2q_0, M_0 - 4q_0, ..., f_{min}$ and we exploiting characteristic of MWC system transfer to calibrate the MWC system.

For the calibration, we consider injecting cosine tones denoted as

$$x(t) = 2A\cos\left(2\pi(k + a_k)f_p(t + \tau_k)\right) \tag{53}$$

where $2A$ is an amplitude, τ_k corresponds to unknown phase information at k-th injected signal, and $0 < a_k < f_p$ is a known off-set frequency. Like as (42), the output of MWC is derived as

$$
\begin{aligned}
y_{i,k}[n] &= \sum_{l=-L_0}^{L_0} \tilde{c}_{i,l} \cdot LPF\{x(t) \cdot e^{-j2\pi f_p l t}\}\Big|_{t=nT_s} \\
&= \sum_{l=-L_0}^{L_0} \tilde{c}_{i,l} \cdot LPF\{2A\cos\left(2\pi(k+a_k)f_p(t+\tau_k)\right) \cdot e^{-j2\pi f_p l t}\}\Big|_{t=nT_s} \\
&= \sum_{l=-L_0}^{L_0} A \cdot \tilde{c}_{i,l} \cdot LPF\left\{\left(e^{j2\pi(k+a_k)f_p(t+\tau_k)} + e^{-j2\pi(k+a_k)f_p(t+\tau_k)}\right) \cdot e^{-j2\pi f_p l t}\right\}\Big|_{t=nT_s} \\
&= \sum_{l=-L_0}^{L_0} A \cdot \tilde{c}_{i,l} \cdot \theta_{i,k}^{k+a_k} \cdot LPF\left\{e^{j2\pi(k+a_k-l)f_p t}\right\}\Big|_{t=nT_s} + \sum_{l=-L_0}^{L_0} A \cdot \tilde{c}_{i,l} \cdot \theta_{i,k}^{-(k+a_k)} \cdot LPF\left\{e^{-j2\pi(k+a_k+l)f_p t}\right\}\Big|_{t=nT_s} \\
&= \sum_{l=-L_0}^{L_0} A \cdot \tilde{c}_{i,l} \cdot \theta_{i,k}^{k+a_k} \cdot e^{j2\pi(k+a_k-l)f_p t}\Big|_{t=nT_s}, \qquad |k + a_k - l| \le \frac{q}{2} \\
&\quad + \sum_{l=-L_0}^{L_0} A \cdot \tilde{c}_{i,l} \cdot \theta_{i,k}^{-(k+a_k)} \cdot e^{-j2\pi(k+a_k+l)f_p t}\Big|_{t=nT_s}, \qquad |k + a_k + l|'''' \\
&= \sum_{l=-q_0}^{+q_0} A \cdot \tilde{c}_{i,l+k} \cdot \theta_{i,k}^{k+a_k} \cdot e^{j2\pi(l+a_k)f_p t}\Big|_{t=nT_s} + \sum_{l'=-q_0}^{+q_0} A \cdot \tilde{c}_{i,-k+l'} \cdot \theta_{i,k}^{-(k+a_k)} \cdot e^{-j2\pi(l'+a_k)f_p t}\Big|_{t=nT_s} \\
&= \sum_{l=-q_0}^{+q_0} A \cdot \tilde{c}_{i,l+k} \cdot \theta_{i,k}^{k+a_k} \cdot e^{j2\pi(l+a_k)f_p t} + \tilde{c}_{i,-k+l} \cdot \theta_{i,k}^{-(k+a_k)} \cdot e^{-j2\pi(l+a_k)f_p t}\Big|_{t=nT_s}
\end{aligned}
\tag{54}
$$

The DTFT of last of upper equation is

$$\mathbf{Y}_{i,k}^{(l)}\left(e^{j2\pi fT_p}\right) = A \cdot \theta_{i,k}^{k+a_k} \cdot \tilde{c}_{i.l+k} \cdot \delta\left(f - a_k f_p\right) + A \cdot \theta_{i,k}^{-(k+a_k)} \cdot \tilde{c}_{i.l-k}\delta\left(f + a_k f_p\right) \tag{55}$$

Denoted as (5), each column and row of $\mathbf{Y}_{i,k}^{(l)}\left(e^{j2\pi fT_p}\right)$ corresponds to output value at f and expanded channel index. From the equation of (55), we can select two column corresponding $f = +a_k f_p, -a_k f_p$ whose values are respectively

$$
\begin{aligned}
\mathbf{Y}_{k}^{(l)}\left(e^{j2\pi fT_p}\right)\Big|_{f=a_k f_p} &= A \cdot \theta_{i,k}^{k+a_k} \cdot \tilde{c}_{i.l+k} \\
\mathbf{Y}_{k}^{(l)}\left(e^{j2\pi fT_p}\right)\Big|_{f=-a_k f_p} &= A \cdot \theta_{i,k}^{-(k+a_k)} \cdot \tilde{c}_{i.l-k}
\end{aligned}
\tag{56}
$$

The algorithm is start with the first injection of pilot cosine tone of $k = M_0$. To equalize the unknown phase information $\theta_{i,k}$, by exploiting $\tilde{c}_{i.-M_0-1}$ and $\tilde{c}_{i.M_0}$ has same value as presented at (24), the two elements of equation of (56) are selected as

$$\mathbf{Y}_{M_0}^{(0)}\left(e^{j2\pi fT_p}\right)\Big|_{f=a_{M_0} f_p} = A \cdot \theta_{i,M_0}^{M_0+a_{M_0}} \cdot \tilde{c}_{i.M_0} \tag{57}$$

The another one is selected as

$$
\begin{aligned}
\mathbf{Y}_{M_0}^{(-1)}\left(e^{j2\pi fT_p}\right)\Big|_{f=-a_{M_0} f_p} &= A \cdot \theta_{i,M_0}^{-(M_0+a_{M_0})} \cdot \tilde{c}_{i.-1-M_0} \\
&= A \cdot \theta_{i,M_0}^{-(M_0+a_{M_0})} \cdot \tilde{c}_{i.M_0}
\end{aligned}
\tag{58}
$$

Consequently, by dividing the last of (58) into (57), the unknown phase information at $k = M_0$ is estimated, such as

$$\frac{\mathbf{Y}_{M_0}^{(0)}\left(e^{j2\pi fT_p}\right)\Big|_{f=a_{M_0} f_p}}{\mathbf{Y}_{M_0}^{(-1)}\left(e^{j2\pi fT_p}\right)\Big|_{f=-a_{M_0} f_p}} \approx \frac{A \cdot \theta_{i,M_0}^{M_0+a_{M_0}} \cdot \tilde{c}_{i.M_0}}{A \cdot \theta_{i,M_0}^{-(M_0+a_{M_0})} \cdot \tilde{c}_{i.M_0}} = \theta_{i,M_0}^{2(M_0+a_{M_0})} \implies \widehat{\theta_{i,M_0}^{M_0+a_{M_0}}} = \sqrt{\frac{\mathbf{Y}_{M_0}^{(0)}\left(e^{j2\pi fT_p}\right)\Big|_{f=a_{M_0} f_p}}{\mathbf{Y}_{M_0}^{(-1)}\left(e^{j2\pi fT_p}\right)\Big|_{f=-a_{M_0} f_p}}} \tag{59}$$

With the estimated phase information, we can estimate system transfer values of $\tilde{c}_{i.M_0-q_0}$ to $\tilde{c}_{i.M_0+q_0}$.

Secondly, by injecting $k = M_0 - 2q_0$ cosine signal, there is a duplicated system value $\tilde{c}_{i.M_0-q_0}$, which is located at

$$\mathbf{Y}_{M_0-2q_0}^{(q_0)} \left(e^{j2\pi fT_p} \right) \Bigg|_{f=a_{M_0-2q_0}f_p} = A \cdot \theta_{i,M_0-2q_0}^{M_0-2q_0+a_{M_0-2q_0}} \cdot \tilde{c}_{i.M_0-q_0} \tag{60}$$

Since we already estimated $\tilde{c}_{i.M_0-q_0}$ at the first step, we can easily estimate the second unknown phase

information $\theta_{i,M_0-2q_0}^{M_0-2q_0+a_{M_0-2q_0}}$. These phase estimation and then acquiring practical system transfer values

are iterate to acquire reach $f_{\min}$.

To verify the success of calibration with proposed method, we artificially make 7 chips delays of PR

sequence for the practical MWC implementation scenario, which is seriously distorted theoretical

system transfer. For the calibration, we injected $30dB$ cosine signals. The Fig. 14 shows support

recovery rate with 3 kinds of system transfer matrix as answer matrix, theoretical, and calibrated matrix.

Note that the answer matrix is generated with the actual PR chip delay. As shown in the simulation

result, the only calibrated system transfer succeed to approach to the performance of answer matrix,

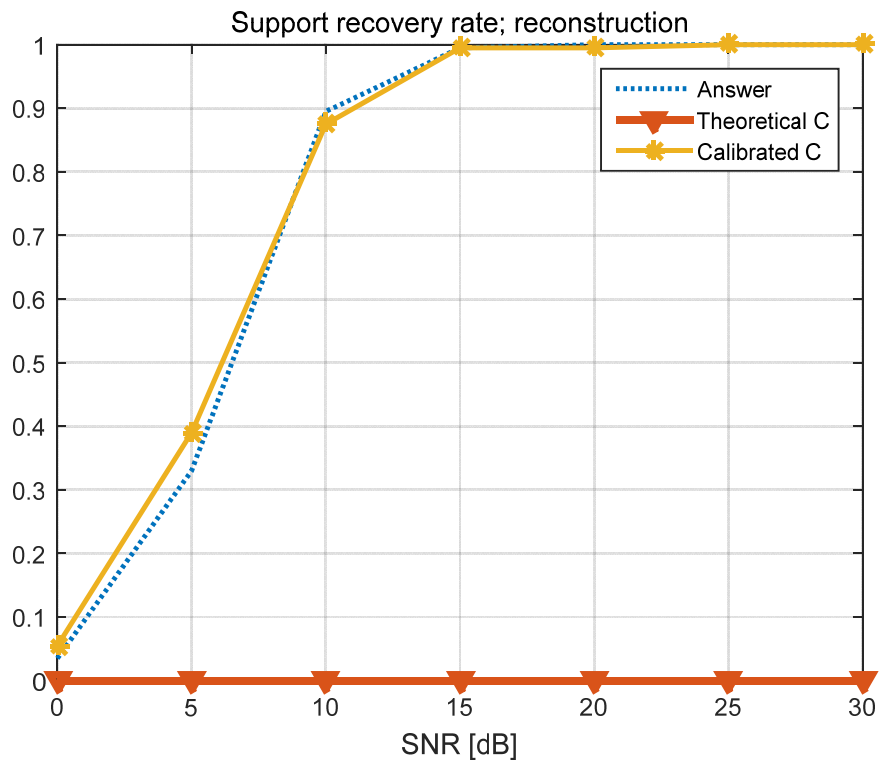while the theoretical matrix failed.

Fig. 15. The calibrated system transfer has similar recovery performance to the actual system transfer (answer matrix).

VI. Conclusion

In this paper, we could verify the signal acquisition performances among the RSSR, RMPI, and MWC with the probability analysis. In that analysis, the MWC showed the better performance than the others. In addition, the analysis might imply that it can be extended to compare with the other CS based sub-Nyquist receivers, which are not discussed. With the MWC, the proposed radar ES system could monitor incoming wideband signals. In the ES system, the zero padding method in the DSP part and integration processing resolved the time aliasing problem. In addition, the signal division scheme and straightforward channel expanding method in the DSP much reduced the computational complexity. Moreover, with the similar the support recovery rate, the low complexity SOMP with sub-sampling method also reduced the complexity. Hence, applying the ES system and the low complexity algorithm to a hardware system that currently developed, contributes to realization. In addition, the proposed calibration algorithms succeeded to simultaneously estimate the practical MWC system transfer and unknown phase information, where the previously unknown phase information should be removed in the calibration. The both of straightforward calibration algorithms once worked after operation of the system, and the estimated system transfer is re-used at every reconstruction. Consequently, through our paper, design of the sub-Nyquist radar receiving system and its before and after were researched.

References

[1] B. Le, T. W. Rondeau, J. H. Reed, and C. W. Bostian, "Analog-to-digital converters," *IEEE Signal Process. Mag.*, vol. 22, no. 6, pp. 69–77, Nov. 2005.

[2] A. B. Carlson, *Communication Systems: An Introduction to Signals and Noise in Electrical Communication*, Internat.2r.e. edition. New York: McGraw-Hill Education, 1986.

[3] D. L. Donoho, "Compressed sensing," *IEEE Trans. Inf. Theory*, vol. 52, no. 4, pp. 1289–1306, Apr. 2006.

[4] E. Candes and T. Tao, "Decoding by Linear Programming," *arXiv:math/0502327*, Feb. 2005.

[5] M. Mishali, Y. C. Eldar, O. Dounaevsky, and E. Shoshan, "Xampling: Analog to digital at sub-Nyquist rates," *IET Circuits Devices Syst.*, vol. 5, no. 1, pp. 8–20, Jan. 2011.

[6] J. A. Tropp, J. N. Laska, M. F. Duarte, J. K. Romberg, and R. G. Baraniuk, "Beyond Nyquist: Efficient Sampling of Sparse Bandlimited Signals," *IEEE Trans. Inf. Theory*, vol. 56, no. 1, pp. 520–544, Jan. 2010.

[7] M. Mishali and Y. C. Eldar, "Blind Multiband Signal Reconstruction: Compressed Sensing for Analog Signals," *IEEE Trans. Signal Process.*, vol. 57, no. 3, pp. 993–1009, Mar. 2009.

[8] M. Yaghoobi, M. Lexa, F. Millioz, and M. E. Davies, "A low-complexity sub-Nyquist sampling system for wideband Radar ESM receivers," in *2014 IEEE International Conference on Acoustics, Speech and Signal Processing (ICASSP)*, 2014, pp. 1788–1792.

[9] J. P. Slavinsky, J. N. Laska, M. A. Davenport, and R. G. Baraniuk, "The compressive multiplexer for multi-channel compressive sensing," in *2011 IEEE International Conference on Acoustics, Speech and Signal Processing (ICASSP)*, 2011, pp. 3980–3983.

[10] H. Sun, W.-Y. Chiu, J. Jiang, A. Nallanathan, and H. V. Poor, "Wideband Spectrum Sensing with Sub-Nyquist Sampling in Cognitive Radios," *IEEE Trans. Signal Process.*, vol. 60, no. 11, pp. 6068–6073, Nov. 2012.

[11] J. Yoo, S. Becker, M. Monge, M. Loh, E. Candès, and A. Emami-Neyestanak, "Design and implementation of a fully integrated compressed-sensing signal acquisition system," in *2012 IEEE International Conference on Acoustics, Speech and Signal Processing (ICASSP)*, 2012, pp. 5325–5328.

[12] J. Yoo *et al.*, "A Compressed Sensing Parameter Extraction Platform for Radar Pulse Signal Acquisition," *IEEE J. Emerg. Sel. Top. Circuits Syst.*, vol. 2, no. 3, pp. 626–638, Sep. 2012.

[13] D. L. Donoho and M. Elad, "Optimally sparse representation in general (nonorthogonal) dictionaries via ℓ1 minimization," *Proc. Natl. Acad. Sci.*, vol. 100, no. 5, pp. 2197–2202, Apr. 2003.

[14] E. Israeli *et al.*, "Hardware calibration of the modulated wideband converter," in *2014 IEEE Global Communications Conference*, 2014, pp. 948–953.

[15] L. Chen, J. Jin, and Y. Gu, "A calibration system and perturbation analysis for the Modulated Wideband Converter," in *Signal Processing (ICSP), 2010 IEEE 10th International Conference on*, 2010, pp. 78–81.

[16] J. Wang and N. Dong, "Channel gain mismatch and time delay calibration for modulated wideband converter-based compressive sampling," *IET Signal Process.*, vol. 8, no. 2, pp. 211–219, Apr. 2014.

[17] Y. K. Alp, A. B. Korucu, A. T. Karabacak, A. C. Gürbüz, and O. Arıkan, "Online calibration of Modulated Wideband Converter," in *2016 24th Signal Processing and Communication Application Conference (SIU)*, 2016, pp. 913–916.

[18] S. Miller and D. Childers, *Probability and Random Processes: With Applications to Signal Processing and Communications*. Academic Press, 2012.

[19] J. A. Tropp, A. C. Gilbert, and M. J. Strauss, "Algorithms for simultaneous sparse approximation. Part I: Greedy pursuit," *Signal Process.*, vol. 86, no. 3, pp. 572–588, Mar. 2006.

[20] A. V. Oppenheim and R. W. Schafer, *Discrete-Time Signal Processing*, 3 edition. Upper Saddle River: Pearson, 2009.

[21] M. Mishali and Y. C. Eldar, "From theory to practice: Sub-Nyquist sampling of sparse wideband analog signals," *IEEE J. Sel. Top. Signal Process.*, vol. 4, no. 2, pp. 375–391, 2010.

[22] G. Schrick and R. G. Wiley, "Interception of LPI radar signals," in *Radar Conference, 1990., Record of the IEEE 1990 International*, 1990, pp. 108–111.

[23] M. Mishali, A. Elron, and Y. C. Eldar, "Sub-nyquist processing with the modulated wideband converter," in *Acoustics Speech and Signal Processing (ICASSP), 2010 IEEE International Conference on*, 2010, pp. 3626–3629.

Acknowledgement

First, thanks to valueless research for a short but precious two years. Although it is regarded as common parlance but it is evidently true, I really want to express my gratitude to direct-indirect helpful previous researchers, my country, GIST, and academic advisor prof. Heung-No Lee and INFONET lab members.